Title
A Light Driven Burst of Hydroxyl Radicals in Newly Formed Cloud Droplets from Reaction Between Iron(II) and Organic Peroxides

Author
Chen, Jie Rou

Publication Date
2019

Peer reviewed|Thesis/dissertation

UNIVERSITY OF CALIFORNIA

Los Angeles

A Light Driven Burst of Hydroxyl Radicals in Newly Formed Cloud Droplets from Reaction Between Iron(II) and Organic Peroxides

A thesis submitted in partial satisfaction of the requirements for the degree of Master of Science in Atmospheric and Oceanic Sciences

by

Jie Rou Chen

2019

ABSTRACT OF THE THESIS

A Light Driven Burst of Hydroxyl Radicals in Newly Formed Cloud Droplets from Reaction Between Iron(II) and Organic Peroxides

by

Jie Rou Chen

Master of Science in Atmospheric and Oceanic Sciences

University of California, Los Angeles 2019

Professor Suzanne E. Paulson, Chair

One of the most uncertain aspects of the climate system are aerosol particles and their interaction with clouds. Aerosol aging in the aqueous phase often involves reactive oxygen species such as hydroxyl radicals (OH), hydrogen peroxide (H_2O_2), superoxide ($O_2^{\bullet -}$), and organic peroxides. In clouds, chemistry driven by hydroxyl radicals is a well-known contributor to production of secondary organic aerosols. OH in cloud and fog droplets originate from various sources, and models currently assume the main source of hydroxyl radicals in clouds is uptake from the gas phase. Work done previously in the group suggested a new, potentially substantial source of OH in cloud droplets when exposed to near UV light.

In this study, we are able to produce similar behavior to field sample observations from mixtures of Fe(II) and peracetic acid (PAA) in the presence of light. We investigate this reaction to see if we can explain the 'OH burst' which occurs within moments of sample preparation. This

is a previously unrecognized reaction and we observe a concentration-saturation effect to the amount of OH produced in the burst.

We observe the OH burst from the reaction of Fe(II) and PAA in 320 nm light and in dark conditions. The reaction in the presence of near UV light immediately produces almost double the OH as the reaction in the dark demonstrating a clear light dependence. This is a possible photo-Fenton like reaction cycling Fe(II) amplifying the OH production. At higher concentrations of Fe(II) and PAA molar yield of OH decreases in both the light and dark conditions, producing less OH per μM of reactant compared to lower concentrations of either Fe(II) or PAA. Inhibition from iron-organic complexes or saturation effects are possibly limiting OH yield at high concentrations of initial reactants.

The thesis of Jie Rou Chen is approved.

Jochen Peter Stutz

Pablo Saide Peralta

Suzanne E. Paulson, Committee Chair

University of California, Los Angeles

2019

Table of Contents

List of Figures

Acknowledgements

I would like to express my gratitude for my incredible advisor, Suzanne Paulson, for supporting me throughout my time here working towards my masters. I am very grateful for her patience and encouragement in areas of research and career aspirations, especially when I felt a little lost. No matter how much she has on her plate, I believe everyone under her guidance feels the deep sense of care she has for each of us, professionally and personally, and I have the utmost respect for her. I look at all her career accomplishments and activeness in the community while kicking butt at being a mother and going rock climbing and realize she is my complete role model. I truly would not have been able to do any of this without her.

I would also like to thank my committee members Jochen Stutz and Pablo Saide for taking the time to be on my committee. They have been very patient, working with me to meet deadlines and offering helpful suggestions and encouragement for my work. I also wanted to thank everyone in the front office and the computer lab for helping me with all my administrative issues, printer problems, and AOS login resets. I am also thankful for Tina Treude for letting us use her deionized water system and also all the professors I was able to take classes with, it was inspiring to be able to learn from the best in the field.

My cohort here at AOS is so special to me. They supported me when I was struggling and always reminded me that I was where I needed to be. For this, I am eternally grateful. A special thanks to David Gonzalez and Michelle Kuang, who were great company in the lab. I could always go to them for guidance and always had a fun time with them outside of the lab. Everyone in this department has such a contagious passion and interest in the work they do. Although the grind is

tough, it was incredible being able to be surrounded by these people the past few years. I can confidently say I am constantly inspired and challenged by the graduate students in AOS.

Finally, I would like to thank my friends and family from Tennessee for always encouraging me to pursue my passions and strive for excellence, even if it meant moving 3000 km away. I have learned so much and gained so many wonderful experiences that I will cherish forever.

1. Introduction

Changes in human activity since the preindustrial era have led to many societal advances. Unfortunately, the associated anthropogenic impacts on aerosols, fogs, and clouds have a significant influence on Earth's climate and air quality through direct and indirect effects. Aerosol particles contribute to climate change through scattering and absorption of radiation by interacting with clouds. Aerosols are processed by cloud droplets, changing aerosol size distributions and chemical composition, and can modify cloud microphysics (Sekiguchi et al., 2003).

Organic material constitutes the largest portion of aerosol mass, with more than half coming from secondary sources formed from reaction in the atmosphere, yet it remains one of the least understood components and is largely under-predicted in current models (Jimenez et al., 2009). Given the importance of secondary organic aerosol (SOA), many studies have focused on the formation pathways and composition of SOA in the field and in lab. Less attention has been given to the reactive properties and how the chemical nature of the particles might change in the atmosphere (Jimenez et al., 2009, Badali et al., 2015). The lack of direct observation and uncertainty in the magnitude of such reactions has led to this area being overlooked in chemistry transport models (Whalley et al., 2015).

Atmospheric free radicals maintain the oxidizing power of the troposphere acting as an important mechanism for the removal of anthropogenic and biogenic primary pollutants. Serious secondary air pollution events can develop due to fast oxidation of primary pollutants (Lu et al., 2018). Hydroxyl radicals often act as the first step in the removal of surrounding organic and certain inorganic species; if these species are not removed by photolysis or wet deposition. Rate of reaction with OH radicals is a key factor in determining the atmospheric lifetime of many of

these organic species (Gligorovski et al., 2015). The hydroxyl radical is the dominant oxidant in the troposphere and has a major impact on the distribution and concentration of pollutants in the atmosphere (Levy 1972, Isaksen and Dalsoren 2011). The hydroxyl radical reacts with virtually all trace species in the atmosphere, and its importance is due to this high reactivity in conjunction with its relatively high concentration sustained through its cycling and regeneration (Seinfeld and Pandis 2016).

In clouds, chemistry driven by hydroxyl radicals is a well-known contributor to production of secondary organic aerosols. The hydroxyl radicals lead to further oxidation of aerosol particles and substantially increase aerosol mass concentrations and distributions of aerosols when the cloud re-evaporates (Abhishek et al., 2016, El-Sayed et al., 2015, Lim et al., 2005, Ervens et al., 2014, Ge et al., 2012). Aqueous OH radicals in cloud droplets also contribute to global sulfate production through the oxidation of climate relevant gases like methane sulfonic acid and dimethyl sulfoxide, intermediate products from dimethylsulfide (DMS) oxidation (Barnes et al., 2006, Hoffmann et al., 2016). In order to assess the relative importance of gas-phase or aqueous phase reactions of OH with atmospheric components, a comprehensive understanding of hydroxyl radical sources and sinks is needed.

OH in cloud and fog droplets originate from various sources. Uptake of OH from the gas phase through diffusion at the surface is considered a dominant source of hydroxyl radicals in cloud and fog droplets. When reacting with atmospheric trace gases, OH is generated in catalytic cycles leading to sustained concentrations during daylight hours. For a globally averaged gas phase OH concentration ($[OH]_g$) of 1.1×10^6 molecules per cubic centimeter (Voulgarakis et al., 2013), a maximum rate of around 2×10^{-9} M s^{-1} is suggested for a 10 µm diameter droplet (Paulson et al., 2019), although the OH gas phase concentration varies by a factor of around 100 through the

diurnal cycle (Finlayson-Pitts and Pitts 2000). The gas phase diffusion into a droplet is governed by the following equation:

$$J = \frac{3D_g}{R_p^2} C$$

Where flux of OH to the drop is represented by J, D_g is the gas phase diffusion coefficient, R_p is the drop diameter, and C is the ambient gas-phase concentration (Seinfeld and Pandis 2016).

In addition to the uptake of gas phase OH radicals into cloud droplets, chemical reactions within the droplets provide another source of OH radicals, via a number of routes (Herrmann et al., 2010). One of these processes is the Fenton reaction, involving the breakdown of hydrogen peroxide by dissolved transition metals such as iron(II) (R1). Here, iron(II) is oxidized by hydrogen peroxide to produce iron(III), with a hydroxide ion and a hydroxyl radical as products.

$$Fe^{+2} + H_2O_2 \rightarrow Fe^{+3} + OH^- + OH\bullet \quad \text{(R1)}$$

Furthermore, photochemical processes also produce OH. In the 'photo-Fenton' reaction, the Fenton reaction (R1) occurs after rapid photoreduction of iron(III) to iron(II) (Zepp et al., 1992). Other mechanisms for OH production within droplets include direct photolysis of hydrogen peroxide (Zellner et al., 1990), iron hydroxides (Deguillaume et al., 2005), nitrate, and nitrite (Zellner et al., 1990).

Other groups have explored OH formation by exposing cloud water samples to simulated sunlight in a laboratory setting with production rates of (0.03-3) x 10^{-10} M/s in the first two hours and no measurable activity under dark conditions (Bianko et al., 2015, Arakaki et al., 1998). This

rate is significantly slower than uptake of OH from the gas phase estimated by the gas phase diffusion equation (Paulson et al., 2019).

Recent work from our laboratory simulated chemistry of newly formed cloud and fog droplets by adding water to ambient aerosol samples with dilution ratios of aerosol to water comparable to that of cloud droplet range. These sample solutions were illuminated at near-UV light conditions and the $[OH]_{aq}$ formation was quantified with fluorescence. Immediately upon illumination, the samples exhibited a large spike of OH production which is referred to as the 'OH burst.'

OH formation was not detected under dark conditions, suggesting a process driven by UV light. It was determined that the initial 9 seconds of light was sufficient enough to photolyze all of the OH-producing chromophores. The rapid increase of OH stops after 2-3 minutes and is followed by a slower, usually linear phase of OH formation in the range expected from processes mentioned earlier (Paulson et al., 2019). Sites in the study were chosen for their different characteristics and implied that the ability of particles to produce the OH burst is widespread among various urban and rural atmospheric conditions. In sites at Claremont and Fresno, the initial burst produced up to 3.5μM OH (Paulson et al., 2019).

The hydroxyl radical burst is not well explained by previously known pathways to OH formation in cloud drops considered earlier, which have rates that are a magnitude of 1-3 orders too slow for the burst exhibited. Laboratory levels of OH and H_2O_2 are low and cannot explain the observed OH. H_2O_2 measured in aerosol extraction solutions was below 2nM at the same time scale of the observed OH burst of a few minutes. The low amounts of H_2O_2 indicate a process other than the Fenton reaction (R1) can better explain the OH burst.

Organic peroxy radicals and peroxides are thought to be important intermediate species in OH cycling (Lelieveld et al., 2008) and in formation of organic aerosols (Paulot et al., 2009). Docherty et al. (2015) indicated that the secondary organic aerosol was predominantly organic peroxides by peroxide analysis, estimating its contribution at approximately 47 and 85% of the SOA mass formed in the alpha- and beta-pinene reactions, respectively, in chamber experiments. Badali et al., (2015) found that photolysis of secondary organic aerosol formed OH at a rate five times faster than photolysis of pure hydrogen peroxide solutions using corresponding H_2O_2 concentrations to peroxide concentrations in the SOA solutions. Comparing OH formation from photolysis of SOA and hydrogen peroxide or organic hydroperoxide solutions, hydrogen peroxide solutions yielded a factor of five smaller whereas organic hydroperoxide solutions resulted in OH formation within a factor of two of the SOA photolysis (Badali et al., 2015). This implies that non-hydrogen peroxide species are photolyzing into OH and further reinforces SOA as a viable source of OH in cloud water, especially given high SOA concentration.

Reactive oxygen species (ROS), including OH radicals, superoxide radicals (O_2^{-}•), hydrogen peroxide (H_2O_2), and organic radicals, exist in the gas and condensed phases and can produce extremely low volatility compounds and highly oxidized molecules largely consisting of these organic hydroperoxides (Tong et al., 2017, Ehn et al., 2014, Riva 2016, Bianchi et al., 2016). Organic hydroperoxides are formed through multiple generations of oxidation or autoxidation and are easily broken down into OH radicals in the condensed phase from UV exposure and under dark conditions (Tong et al., 2017, Badali et al., 2015). Tong et al. (2015) determined that presence of dissolved iron atoms in the form of mineral dust can enhance OH production due to Fenton-like reactions (R2, R3) with organic hydroperoxides. They believe this aging and decomposition of

SOA in cloud or fog droplets is comparably important to production of OH from the classic Fenton reaction (Tong et al., 2015).

$$Fe^{2+} + ROOH \rightarrow Fe^{3+} + RO\bullet + OH^{-} \quad (R2)$$

$$Fe^{2+} + ROOH \rightarrow Fe^{3+} + RO^{-} + OH\bullet \quad (R3)$$

Peroxyacetic acid or peracetic acid (PAA) is an organic hydroperoxide that plays a potentially important role in atmospheric processes as a reservoir of free radicals and can reflect the free radical levels of the troposphere (Zhang et al., 2010). No significant direct emission of PAA from natural or anthropogenic sources has been found. It is believed that PAA in the atmosphere is mainly produced through combination of peroxy radicals (Lightfoot et al., 1992, Staffelbach et al., 1995) or reaction of acetyl peroxy radical with high concentrations of compounds such as formate, formaldehyde, glyoxal and phenolic compounds, which are "H-atom donors" commonly found in the aqueous phase (Faust et al., 1997). Lind et al. (1987) determined the Henry's law constant for peracetic acid to be 467.6 M atm^{-1} and an aqueous phase concentration ranging between $1x10^{-6}$ M to $1x10^{-4}$ M (Lind et al., 1987), although peracetic acid will partition mostly toward the gas phase.

In this study, we investigate the reaction of peracetic acid with iron(II) in the presence of light to see if we can explain the 'OH burst' in simulated cloud water from field samples. We suggest a potentially substantial source of OH formation in clouds from unrecognized chemistry between iron(II) and peracetic acid (PAA) in the presence of light. We explore this chemistry and the concentration dependences of the constituents with possible inhibitory effects as well as an observed Fe(II)-PAA ratio dependence.

2. Materials and Methods

Peracetic acid (PAA) (32% wt), Iron(II) sulfate heptahydrate (≥ 99%, reagent grade), 2-hydroxyterphthalic acid (≥ 97%) (hTA), phosphoric acid (≥ 99.999%), Iron(III) chloride hexahydrate (97%), ferrozine (3-(2-Pyridyl)-5,6-diphenyl-1,2,4-triazine-p,p'-disulfonic acid monosodium salt hydrate), and nitric acid (70%, trace metal grade) were all purchased from Sigma-Aldrich. Disodium Terephthalate (≥ 99%) (TA) was purchased from TCI America. Sulfuric acid (reagent grade, 0.1N) was purchased from Titripur. Sodium phosphate dibasic, potassium phosphate monobasic were purchased from Acros (reagent grade). Acetonitrile (HPLC grade) was purchased from OmniSolv. Methanol (HPLC grade) was purchased from Fisher Chemical. All materials were used as received.

Peracetic acid, Iron(II) sulfate, Iron(III) chloride, TA, and sulfuric acid were used for sample preparation. hTA was used for the calibration standards. Ferrozine and hydroxylamine were used for UV absorption and the Ferrozine assay with the LWCC. Phosphoric acid, sodium phosphate dibasic, and potassium phosphate monobasic were used to make the phosphate buffer for the HPLC eluent. Acetonitrile and methanol were used during HPLC analysis. Nitric acid was used for acid washing.

2.1 Solution Storage and Cleaning Procedure

Iron stock solutions were prepared from 10^{-2} to 10^{-4} M in 60 mL Teflon containers. Peracetic acid stock solutions and all sample solutions were prepared in glass vials. Stock and sample solutions were prepared in 18 MΩ deionized Milli-Q water acidified to pH 3.5 using 0.1 N sulfuric acid.

hTA stock solution 10^{-3} M was wrapped in foil and refrigerated for a few months, remaining stable in solution over this time frame. Fe(II) and PAA stocks were prepared daily because their absorption spectra and ability to produce OH decreased if kept longer than a day, suggesting breakdown in solution. The following describes preparation procedures.

All glassware and Teflon containers were cleaned with the following procedure: washed with warm water and soap, rinsed with DI water (3 x), ethanol (3 x), and DI water again before being filled with 1 M nitric acid and left overnight. They were then rinsed with DI water (3 x) again and placed upside down to air dry.

2.2 Detailed Stock Solution Preparation

Finnpipette II (Fisherbrand, 20-200µL), Finnpipette (Fisherbrand, 40-200µL), and Eppendorf pipettes (5.0mL) were used for all stock and sample preparation. Ohaus PA163 Pioneer analytical/precision balance (1 mg readability) was used to weigh all solid samples and weighing paper was tared before each measurement.

Prepared daily:

Iron(II): For 10^{-2} M iron(II) stock, 0.0278 g of $FeSO_4 \cdot 7H_2O$ was weighed on weigh paper and transferred to a 60 mL Teflon bottle. 10mL of pH 3.5 was added and solution mixed. 100µL of the stock 1 solution was added to 9.900 mL of pH 3.5 for dilution to 10^{-4} M (stock 2). Stock 2 was used directly for sample preparation.

$$0.0278\ g * \frac{1mol}{278.01g} * \frac{1}{10mL} * \frac{1000mL}{1L} = 10^{-2} M\ Fe(II)$$

Dilutions were calculated using $C_1V_1 = C_2\ V_2$, where *X* is the volume (V_2) needed of stock 1 to prepare stock 2.

$$Dilution\ to\ Stock\ 2: \ \ 10^{-4}M * 10\ mL = 10^{-2} * X\ mL = \mathbf{100\mu L\ of\ stock\ 1\ in\ 10\ mL}$$

Peracetic acid (PAA): For 10^{-2} M peracetic acid (stock 1), 21 µL of 32% wt peracetic acid was pipetted into 9.980 mL of pH 3.5 solution. This was diluted to 10^{-4} M (stock 2) and used directly.

$$32\%\ wt\ PAA\text{: } \frac{32g}{100g} * \frac{1\ mol}{76.05g} * \frac{1.13g}{mL} * \frac{1000mL}{1L} = 4.75M\ PAA$$

$$Stock\ 1\ preparation\text{: } 10^{-2}M * 10\ mL = 4.75\ M * X\ mL = 21\mu L\ of\ 32\%\ wt\ PAA\ in\ 10\ mL$$

Prepared as needed:

pH3.5: 3.16mL of 1N (0.5 M) H_2SO_4 was added to a 500mL glass cylinder filled with deionized water. This was poured into the polyethylene storage bottle, and another 500 mL of water was added for 1 L total of solution.

$$pH = -\log[H^+]$$

$$[H^+] = 10^{-3.5}M = 3.16 * 10^{-4}\text{M}$$

$$0.1N * V = 3.16 * 10^{-4} * 1000mL = 3.16\ mL\ H_2SO_4$$

The pH was checked with a Hanna Instruments (HI 3220) benchtop pH meter. The meter was calibrated with each use, using standardized buffers from Fisher Chemical (pH 4.0, 7.0 and 10.0).

The probe electrolyte level was checked and filled through fill hole screw if needed. The probe was first rinsed with deionized water, and then placed in a small glass vial with buffer solution until the pH reading stabilized. Between calibration points, probe was rinsed with deionized water and patted gently with a KimWipe only if needed. Temperature was manually input and buffer solutions were poured fresh each week as equilibrium with atmospheric conditions can change the pH of standard solutions. Once finished, probe was rinsed with deionized water and stored in provided cap with a few drops of Hanna Instruments storage solution (HI70300) to maintain condition of the probe.

100mM Terephthalate: 0.5252 g $C_8H_4Na_2O_4$ weighed and transferred to amber bottle. 25mL pH 3.5 added and shaken vigorously until the solid dissolved.

$$0.5252g * \frac{1mol}{210.10g} * \frac{1}{25mL} * \frac{1000mL}{1L} = 10^{-1}M\ TA$$

2-hydroxyterephthalic acid (hTA): A 10^{-3} M stock solution was made by dissolving 0.0055 g of 2-hydroxyterephthalic acid (hTA) into 30 mL of pH 3.5 in a teflon bottle wrapped in aluminum foil and stored in the fridge and remade every few months. For the hTA calibrations, a 10^{-5} M stock was prepared by performing a 1:100 dilution from 10^{-3} M stock.

$$0.0055g * \frac{1mol}{182.13g} * \frac{1}{30mL} * \frac{1000mL}{1L} = 10^{-3}M\ hTA$$

The following table shows the amounts used for the desired concentrations of standard solutions in our eight-point calibration curve. This was performed daily before experiments were conducted. The fluorescence spectrometer made three readings in succession which were averaged.

8 point hTA Calibration curve:

[hTA] (nM)	Volume of 10^{-5} M hTA (µL)	Volume of pH 3.5 (mL)
50	25	4.975
100	50	4.950
500	250	4.750
800	400	4.600
1000	500	4.500
1500	750	4.250
1800	900	4.100
2000	1000	4.000

2.3 Generation and Quantification of OH Radicals

Each sample solution contained an excess (10mM) sodium terephthalate, which reacts with the OH radical to produce a strongly fluorescent 2-hydroxyterephthalic acid (hTA) with a 31% yield in pH 3.5 (Gonzalez et al., 2018) shown in the mechanism below. hTA was detected at excitation/emission wavelength (λex/λem) of 320/420 nm measured in single-wavelength mode with 10nm slit widths and 30 ms integration time using the Lumina Fluorescence Spectrometer (Thermo Scientific). An eight-point calibration of hTA (50-2000 nM) was performed before each experiment. All samples were measured in microcuvettes, cleaned with water and ethanol and dried. Once a contamination issue was detected in measurements, a more thorough cleaning of the microcuvette was adopted in which the microcuvette was filled with 1M nitric acid (HNO_3) for a few hours every two weeks to remove any contaminants.

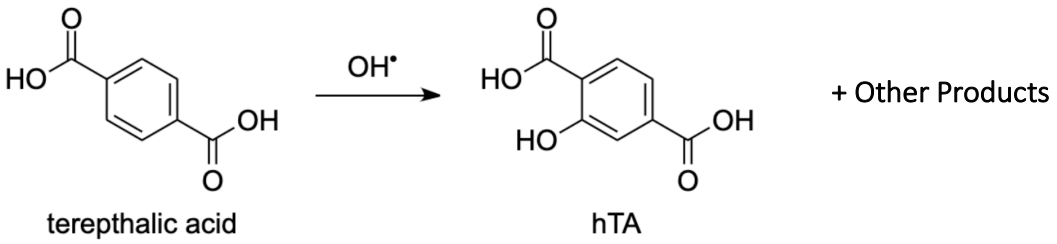

The TA and peracetic acid were added to pH 3.5 in a glass vial and mixed by shaking; $FeSO_4$ was added last to initiate the Fenton reaction and immediately covered with Parafilm. Immediately after mixing, a 200 µL aliquot of the sample was taken from the sample vial and placed in the fluorometer cell holder and exposed to 320 nm light in increments of 9 seconds after pressing the start button. Because the instrument made three consecutive readings, the sample would be exposed to 27 seconds of light. As soon as the third measurement was finished, we prompted another three readings to be measured by pushing the start button again without removing the microcuvette. This was done continuously for up to 216 total seconds of light exposure. For each reading, the signal for fluorescence intensity was measured and recorded. The amount of OH produced throughout the experiment with a light source was calculated using the fluorescence intensity, hTA calibration curve, and hTA yield. Multiple controls were run for each experiment to test for presence of contamination and to account for background OH production not due to the experimental reactions; these included a mixture of only pH 3.5 and TA, and then with the addition of varying amounts of peracetic acid and iron separately.

Quantification of OH without a light source (dark conditions) was performed using a High Performance Liquid Chromatograph (Shimadzu LC-10Ai liquid chromatograph) equipped with a fluorescence detector (Shimadzu RF-10AXL detector). The eluent was delivered at 0.6 mL/min to

a C18 guard column. Eluent for detection of hTA using this method were 70% pH 3 phosphate buffer (with 10% acetonitrile) and 30% methanol, degassed with a steady stream of helium. OH with and without light exposure were measured simultaneously using this method in conjunction with the above in-light portion of the experiment by injecting the sample into the HPLC system every 1-2 minutes. Retention time for hTA using only the guard column was 1 minute and detected at the $\lambda_{ex}/\lambda_{em}$ of 320/400nm. The 100µL syringe used was rinsed with water three times in between experiment runs and washed once with sample solution before injection. Peaks were integrated, and area was used to calculate the OH formation using the hTA calibration.

Varying concentrations of Fe(II) and PAA were reacted, ranging between 1-10 µM at 1 µM increments. Each set of experiments was completed multiple times and often occurring on different days, focusing mostly on 1, 5, and 10µM PAA concentrations with all ten Fe(II) concentrations. An example of sample preparation is shown in the table below.

Experiment	**Total Solution Volume (mL)**	**Volume of pH 3.5 (mL)**	**Volume of 10^{-5} M hTA (µL)**	**Volume of 10^{-4} M PAA (µL)**	**Volume of 10^{-4} M Fe(II) (µL)**
5µM Fe(II) + 5µM PAA	5	4.000	500	250	250
5µM Fe(II) + 5 µM PAA	10	8.000	1000	500	500
1µM Fe(II) + 10µM PAA	5	3.950	500	500	50

2.4 Measurement of UV Absorption

UV absorption was measured for the reactants Fe(II) and PAA in the sample, a mixture of the two, and Fe(III) to see their characteristic spectra in the UV range. UV absorption spectra were measured with a liquid waveguide capillary cell (LWCC-3100, World Precision Instruments Inc.), a UV-Vis light source (AvaLight-DHS, Avantes), and a UV-Vis spectrometer (AvaSpec 2048L, Avantes). The deuterium lamp was used as the UV light source and software was set to 'scope mode'. A 3 mL syringe was used to slowly inject water into the cell 3 times to flush the system. Air bubbles moved to the tip of the syringe by flicking and then pushed out to prevent any air bubbles from being forced into the cell. A 1:5 Contrad cleaning solution to deionized water was used to clean the cell, followed by flushing with more water. Solvent (pH 3.5) was then injected. The spectrum was then referenced with the pH 3.5 and a dark reference was measured with the shutter off and switched to 'absorbance mode'. After this, the sample was injected. The spectrum stabilized within 2 mL of injection and was saved. The syringe was rinsed with water a few times, and then the cell was flushed with pH 3.5 until the baseline returned to zero. This was repeated for the rest of the samples. When finished, the cell was flushed with water and the syringe was left plugged in with water. Further details on software use are in instrumentation guide below.

Preparation of Fe(III): Because of the hygroscopic nature of $FeCl_3 \cdot 6H_2O$, the Fe(III) concentration was obtained indirectly using the Fe(II)-Ferrozine method (Stookey 1970). A four-point Fe(II)-Ferrozine calibration between 20 to 750 nM Fe(II) was performed with addition of 100 µL ferrozine to each 10 mL total solution. A set of three solutions of approximately 300 nM Fe(III) were made by serial dilution. In the Fe(III) solution, 100 µL (10 µL for every mL of total solution) of hydroxylamine (NH_2OH) was added and left for 20 minutes to reduce all Fe(III) to Fe(II), and

100 µL of ferrozine was added to bind up all Fe(II) in solution so it could be measured using the halogen lamp for visible light as a light source. Absorbance at 700 nm (A_{700}) was subtracted from A_{562} to account for instrument drift. The absorbance of the triplicates was averaged and used for back calculation with the dilution factor to get the true concentration of "300 nM" Fe(III). This was then used to calculate the concentration of the stock solution and the desired Fe(III) solutions could be calculated and made from this.

Fe(II)-Ferrozine Method Adjustments:

It was originally thought that ferrozine would immediately bind up Fe(II) in solution. A set of Fe(II)-Ferrozine standards were made for a calibration curve and measured immediately after they were prepared, with ferrozine addition being the last step. The standards were then measured periodically over the next 15 minutes. The corresponding calibration curves are shown in Figure 1 below, accompanied by the best fit equation and R^2 in Table 1. At time 0, when the standards are prepared and immediately measured, it does not appear that the ferrozine has had sufficient time to bind up all the Fe(II). A linear relationship between the standards is seen better when the standards are left for 3-4 minutes before being measured. Calibration curves after 8 minutes are all very similar. When using the Fe(II)-Ferrozine method, samples should be left after addition of ferrozine for at least 3 minutes to allow time for Fe(II) to be bound.

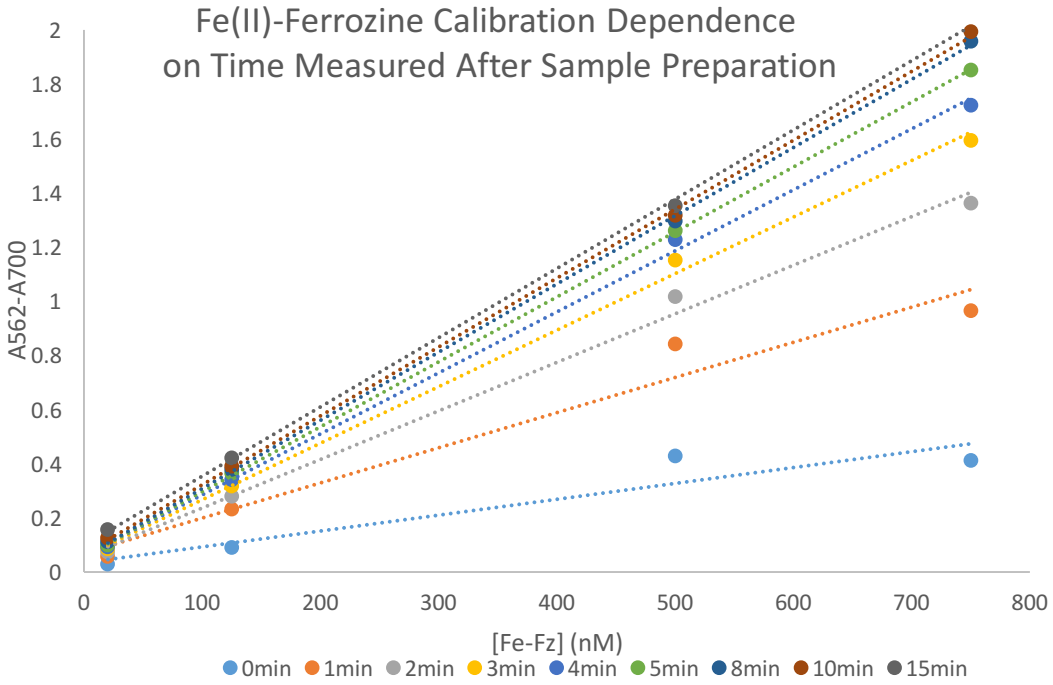

Figure 1. Fe(II)-Ferrozine calibration curves with dependence on time between addition of ferrozine to standards (last step in standard or sample preparation) and measurement of the standards.

Table 1: Fe(II)-Ferrozine calibration curve equations and R^2

Time measured after standard preparation	Fe(II)-Ferrozine Calibration Curve	R^2
0	y = 0.0006x + 0.0343	0.88857
1	y = 0.0013x + 0.0699	0.96149
2	y = 0.0018x + 0.0563	0.99469
3	y = 0.0021x + 0.0574	0.99759
4	y = 0.0023x + 0.0588	0.99855
5	y = 0.0024x + 0.0558	0.99995
8	y = 0.0025x + 0.0569	0.99970
10	y = 0.0025x + 0.0670	0.99958
15	y = 0.0026x + 0.0974	0. 99951

2.5 Techniques

Pipetting: The appropriate size pipette should be chosen for the volume needed to be dispensed. If possible, the desired volume will fall within the volume range of the pipette to minimize error, while also being the smallest pipette suitable for the job to improve accuracy of the volume. For example, if 800 µL is needed, the 1 µL pipette should be used instead of the 200 µL or 5 mL pipettes. Use the correct pipette tip, and pre-wet the tip by aspirating (drawing up) and expelling the solution to coat the inside of the tip and ensure the correct volume is being dispensed. This step is particularly important if the temperature of the solution is colder.

The standard method of pipetting was used in these experiments: the plunger was pressed to the first stop, then the tip was vertically submerged a little below the solution's meniscus, followed by a steady release of the plunger to make sure no air bubbles entered the tip upon aspiration. The pipette was then removed vertically from the solution and dispensed into the second solution by pressing the plunger fully to the second stop. Reverse pipetting can be used if the solution being used is highly volatile.

Consistency in pressure, speed, and aspiration/dispensing angles should be maintained to improve accuracy and precision of the volumes pipetted. Watch for air bubbles or extra liquid on the outside of the pipette tip which can affect the volume. Water was used with the analytical balance to check pipetting methods and can also be used to determine if a pipette needs to be recalibrated.

Mixing: To reduce scatter between trials, a study on sample mixing was performed. During experiments, the Fe(II) required for a sample was always pipetted from a 10^{-4} M stock solution into the solution containing pH 3.5, TA, and PAA. These are both colorless solutions. For some

concentrations of Fe(II) needed, multiple aliquots of the stock solution would be required. It was hypothesized that upon injection of Fe(II), an interface was formed between the two solutions briefly before the solution was mixed. At this interface, the Fe(II) concentration would be much higher than intended without having been diluted by mixing yet, and the fast occurring reaction between Fe(II) and PAA could be enhanced.

This was tested with a simple visual analysis using coloring agents. A vial containing a red solution represented our pH 3.5 PAA mixture, and 800 µL (4 aliquots of 200 µL) of blue solution was added. Images from the video recording are shown below. When dispensing, pipette was held at an angle, and the blue solution either made contact with the vial wall or the surface of the liquid. The blue solution clouded at the top and dispersed into the rest of the solution at a very slow rate. Addition of all aliquots took approximately 10 seconds. Complete mixing did not occur until vial was shaken.

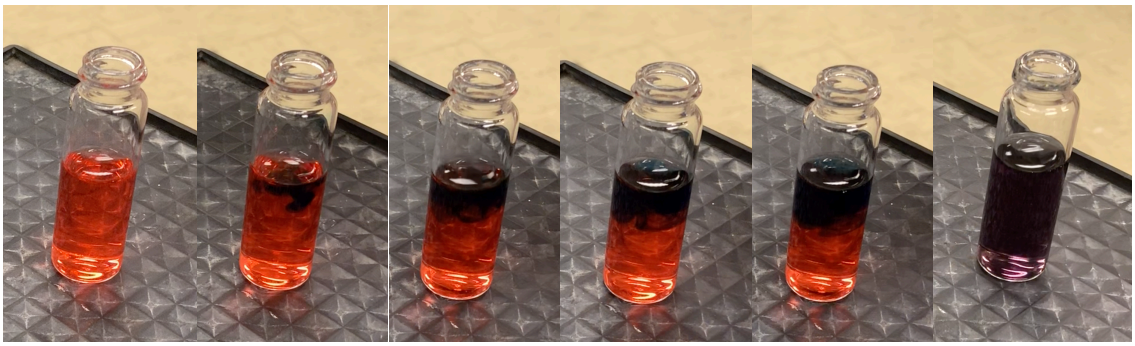

Figure 2. Mixing study done with color agents. First image shows initial solution representing PAA, other pictures show addition of 4 aliquots of 200 µL of a blue solution by pipetting. Last image is solution after it was covered with Parafilm and mixed by shaking. Pipette was held so tip was at an angle when blue solution was expelled.

The use of a Teflon petri dish with constant mixing via gentle agitation at 100 rpm on a shaker (Heidolph, Rotamax 120) was considered to deliver the Fe(II) in a manner that would allow immediate mixing upon pipetting. At this speed, there was still a clear separation between the two solutions and complete dispersion to a well-mixed state took longer than the process in a vial.

The mixing study was performed again in the vial with adjustments in pipetting technique. It was found that when holding the pipette vertically to expel, the blue solution entered with a force that went straight towards the bottom of the vial and created a small scale circulation that caused immediate dispersion and mixing of the solution. There was no pooling or clear interface between the red or blue solutions as opposed to when the pipette tip was held at an angle into the vial.

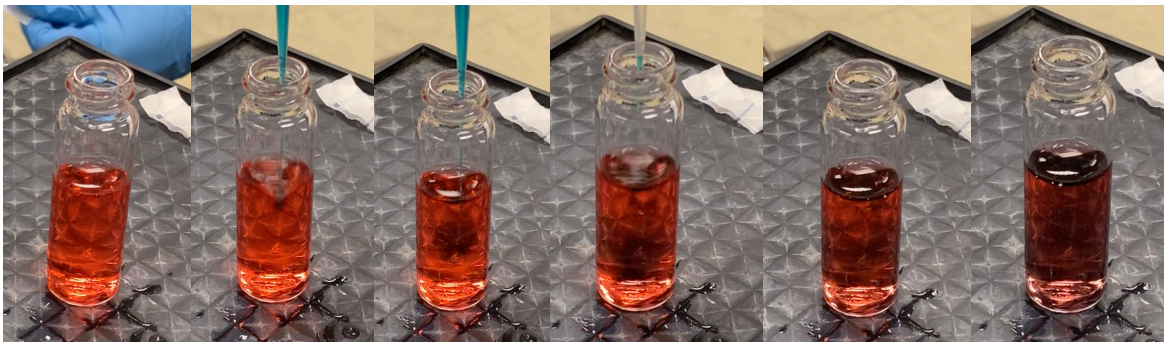

Figure 3. Mixing study with pipette dispensing vertically into solution. First image is before any addition, the next four images show the immediate dispersion and mixing as the first 200µL being dispensed. Last image shows solution immediately after the last aliquot has been added.

There is a clear difference in mixing between pipetting vertically or at an angle. After this study, samples were prepared with pipetting technique adjusted to be in the vertical orientation for consistency. Total solution volumes were scaled down so the amount being pipetted would fit the range of pipettes used when necessary. The figure to the right illustrates immediate mixing with the pipette tip oriented vertically.

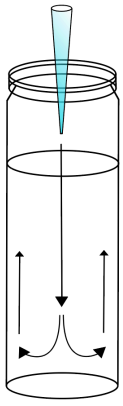

Figure 4. Mixing in vial with pipette held vertically over solution surface

2.6 Instructions for Instrumentation Use

2.6.1 Lumina Fluorescence Spectrometer*:* Power should be turned on from the back of the instrument first before turning on the front power switch. Then, beside the power switch on the

front turn on the control board (red), and lamp (white) in this order to avoid damage to the lamp or control board. Let the instrument warm up for 20 minutes before using. To use the Simple Read software, first open and name a new file and then set parameters. Make sure the parameters set have updated at the top of the window before beginning readings (wavelengths, integration time, slit widths etc.). When finished, turn the instrument off in the reverse order (white and then red) and let the lamp cool for 20 minutes before turning the main switches off.

Decrease in Fluorescence Signal Intensity: Multiple experiments for generation of OH from Fe(II) and PAA were performed each day. We noticed that experiments near the end of the day sometimes yielded less OH than anticipated. It was suspected that the intensity of the fluorescence signal was decreasing slowly over the course of the experiments, which would generally involve having the fluorometer's lamp on for 3-5 hours at a time. To test this, one of the standards from the hTA calibration curve (1000 nM hTA) was measured periodically in between experiment runs. We prepared a new stock solution of hTA to rule out the possibility of solution degradation causing the decrease in fluorescence. Both the old and newly prepared hTA exhibited a decrease in signal intensity over a few hours. Results from freshly prepared hTA are shown below. From the same day, the full range of standards were measured before and after conducting the experiments.

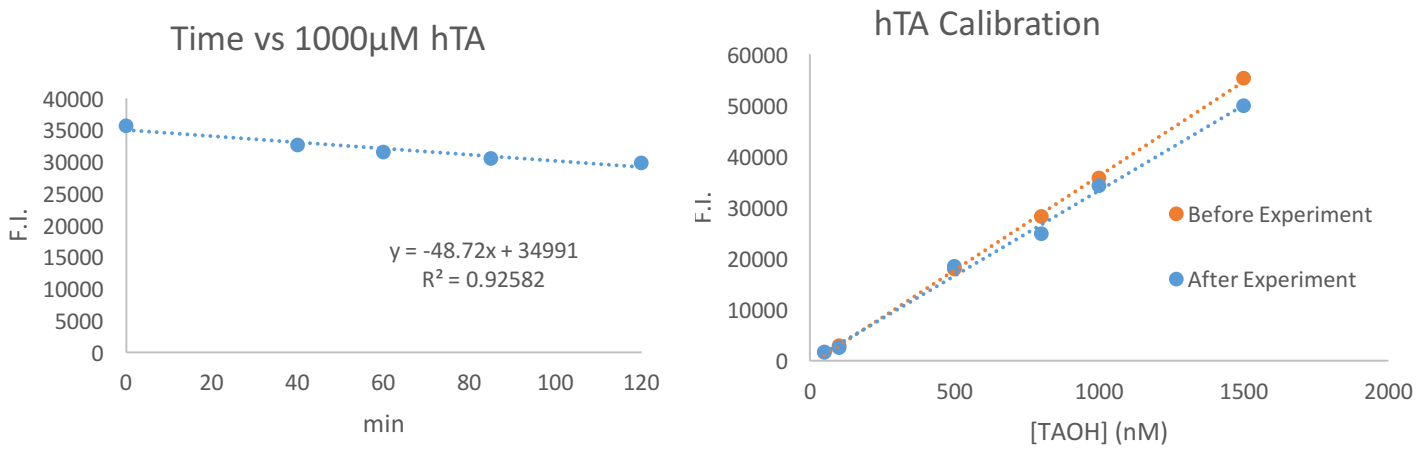

Figure 5. Decrease in fluorescence intensity shown by measurement of 1000 nM standard throughout the day (left) and a before-after full calibration curve. Lamp had been on for 3.5 hours.

The decrease in signal over time could be due to the new lamp that was installed, but we are not certain of this. Data were corrected for the drift in calibration curves and decrease in signal intensity. Possibility of calibration drift and decreasing signal should be kept in mind for future experiments.

***2.6.2 HPLC**:* Turn on Shimadzu LC-10Ai and flush system with a mixture of 95% deionized water and 5% acetonitrile for 20-30 minutes or 15 mL. The system should then be purged with the chosen eluent by first turning off the pressure and letting it drop to 0, removing the suction filter line from the water solution and placing the line into the new eluent, opening the drain valve, and then pressing purge. It is important to ensure that the suction filter is placed with enough liquid for it to be submerged so no air is taken in by the system, which is very sensitive to air bubbles. Once purging is finished, close the drain valve and let the system flush with the eluent by turning on the pump until signal has stabilized.

Eluent should be covered and degassed with a steady stream of compressed helium to remove dissolved oxygen that can result in oxidative degradation of sample and mobile phases as well as to reduce erratic pump delivery of solvent from pressure fluctuations. The detector should be turned on and warmed up for 20-30 minutes until the signal is stable when flushing with eluent. The detector may be zeroed multiple times so that when the chromatograph begins, the baseline is around zero. From the Shimadzu LC-10Ai instruction manual, this pump uses pressure units in kilograms of force per square centimeter (kgf/ cm^2), although no unit of measurement is shown on the display. The pressure on the pump should be mostly stable, but fluctuations within ± 5 kgf/cm^2 is okay.

Before beginning sample measurements, water should be injected into the system a few times, followed by injection of the sample solvent (pH 3.5 solution) as contamination controls, as this method is very sensitive and susceptible to contamination. To inject, turn the injection valve up (counter clockwise), load sample with the syringe, then twist the valve back down to the starting position to inject. Once the experiment is finished, turn the pump pressure off and switch the suction filter line back to the water solution and purge the system again by opening the drain valve and pressing purge. After purging is complete, turn the pump back on and flush the system with this water/acetonitrile mixture for 20 minutes to ensure the eluent is removed from all the lines. This is important so there is no build up or precipitation and also protects the lines from any bacterial growth or microbial (fungal, mold) growth. Bacterial growth can happen with buffers that are too old and should be inspected; if the buffer solution appears cloudy when shaken, prepare a new buffer solution.

Be attentive to the pressure reading and the noisiness of the baseline as these are key indicators of a proper working system; pressure too high can mean there is build-up or precipitate

in the column or somewhere in the system and can cause damage to the lines. If pressure is high, the flow of mobile phase can be checked at different connection points in the system- before or after the analytical column, before the detector, with and without the guard column, or any other points. In ten minutes, the system should elute 6 mL flowing at 0.6mL/min. Watch lines to make sure no air bubbles are being drawn through the lines and never leave the suction filter exposed to the air; air bubbles often result in a jump in the pressure or in the fluorescence signal. Checking for leaks can indicate any damaged parts that may need to be adjusted, cleaned or replaced.

Eluent should be remade every two weeks especially if a phosphate buffer is present because a can precipitate can form over time. Although eluents were not filtered in these experiments, it should be a consideration for the future. Water reservoirs and the system's lines can also harbor bacterial or microbial growth from exposure to laboratory air. The deionized water mixture (95% water, 5% acetonitrile) should be replaced weekly because of the possible bacterial/microbial growth that can harm the system. Lines should always be connected and left with a non-buffered mobile phase in them (water/acetonitrile mixture).

For a more thorough cleaning of the system, it can be flushed with 25mL methanol; this is good to do every once in a while especially if using an analytical column. If needed, lines to the detector can be disconnected and a 3mL syringe can be used to manually flush the detector inlet. If high pressure on a column is not lowered after this, a guide can be found in the instruction manual for a more thorough cleaning (with acetone, water, HNO_3, water, and then eluent). The analytical column can also be placed in the opposite orientation so it can be back-flushed, but it should not be connected to the detector and should not be done often due to the risk of damaging the particles in the column and ruining its integrity. Manuals and online resources were used for more detailed guides on maintaining the health and quality of the HPLC system and methods.

2.6.3 LWCC with Avasoft 8 Software*:* Turn on Avantes AvaLight-DHS light source, then turn on the halogen lamp for visible (in the Fe(II)-Fz method) or the deuterium lamp for UV light, then switch open the shutter. Open Avasoft 8 software, click create new experiment, make a new folder and name the file. Then click the start button on screen and switch to scope mode (appears as an 'S' button). With the syringe, rinse the cell a few times with water paying attention to not inject any air bubbles and do any cleaning procedures if needed. Inject the solvent (pH 3.5) until the spectrum has stabilized. Turn the shutter off and click 'Dark' for a dark reference, then switch the shutter back to open and click 'Reference.' Switch from scope mode back to absorbance mode, which should be a flat line now. Inject sample and once spectrum has stabilized, click 'save' and comment the sample name, then save file. Run the rest of the samples needed, making sure to inject pH 3.5 (or whatever solution was used as reference) and the baseline returns to zero. Once finished, flush the cell with water and leave the syringe plugged in until the next use. Click 'stop' on the screen. Go to 'file', and click 'convert to', 'excel', 'absorbance mode', and highlight all samples needed, which should appear in the file that was made according to the comment for each sample. The software will then export an excel file with the absorbance spectra and corresponding wavelengths.

3. Results and Discussion

With mixtures of peracetic acid (PAA) and Fe(II) illuminated with near UV light, we are able to produce very similar behavior to what was observed in field samples. The reaction results in a rapid burst of OH production in the first minute in both light and dark conditions, where exposure to 320 nm light results in approximately double the magnitude of the burst. The detailed reaction mechanism of

OH formation of Fe-PAA in the dark is unknown, but is maybe similar to the Fenton reaction (R1) with PAA instead of H_2O_2, following the general organic hydroperoxide reaction shown in equation (R2):

$$Fe^{+2} + CH_3C(O)OOH\ (PAA) \rightarrow Fe^{+3} + OH + CH_3C(O)O^- \quad (R4)$$

Exposure of the reaction to near UV light yields substantially higher OH compared to dark conditions for all Fe(II)-PAA concentration ratios. This higher OH yield might be due to photo-Fenton-like reactions in which Fe(III) and organic ligands complex, leading to reduction of Fe and an organic radical which can go on to form OH.

$$Fe^{+3} + CH_3C(O)O^- + h\nu \rightarrow Fe^{+2} + CH_3C(O)O\bullet \rightarrow OH\bullet \quad (R5)$$

The widely varying reaction kinetics of Fe(II) with PAA and H_2O_2 are also observed in other redox systems involving transition metals and organic ligands, and largely depends on the specific metal-ligand pairing (Gonzalez et al., 2017, Welch et al., 2002).

3.1 Concentration and Light Dependence of OH Formation from Peracetic Acid and Fe(II)

Figure 6 below shows the reaction between 1μM Fe(II) and 1μM PAA in dark conditions and illuminated under near UV light (320 nm) over a fifteen-minute time period. Blank solutions omitting either Fe(II), PAA, or both were run for the length of the experiments as controls to account for background OH formation and to check for presence of contamination. In both light and dark conditions, the initial burst of OH production is seen with the first measurement which was taken within the first minute of the reaction starting. In the dark at 1:1 μM Fe:PAA, OH

formation is approximately stoichiometric. With exposure to light, the magnitude of the initial burst is about twice as high. This phenomenon requires both Fe(II) and PAA in the solution. In blank and control experiments in the dark, OH formation is below the detection limit (~20 nM). The same blank experiments conducted in the presence of light show only slightly higher OH formation with a small intercept (usually less than 100 nM) followed by a slow, small linear increase, and is largest for Fe(II) solutions consisting of only Fe(II) and the OH probe in pH 3.5. The Fe(II) control was used as the blank for the data in Figure 6. Mixture of 1 µM Fe(III) and 1 µM PAA in 320 nm light does not exhibit the same characteristic OH burst observed by the system with Fe(II) and PAA.

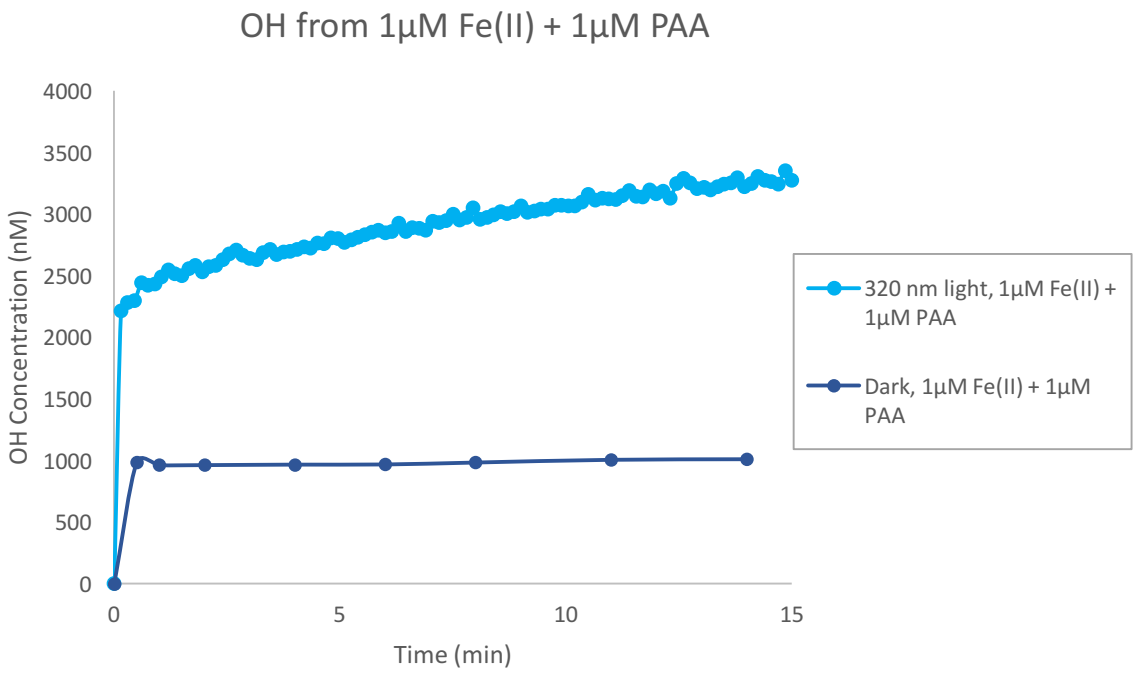

Figure 6. OH formation vs. time from mixtures of peracetic acid (PAA) and Fe(II) in both light (320 nm) and dark conditions. The reaction kinetics observed in the laboratory system closely mimics the OH formation kinetics from field samples shown done previously Paulson's group.

Absorption spectra between 240 – 420 nm are shown in Figure 7 for Fe(II), Fe(III), PAA and mixtures of PAA and Fe(II) in concentrations between 3 and 5 µM in pH 3.5 solution. All spectra were measured in the dark 2 ± 0.5 minutes after mixing. PAA and Fe(II) have weak absorptions in the region, while Fe(III) absorptions are much stronger which is consistent with earlier studies (Orlando et al, 2003; Brigante et al, 2015). The mixture of 1:1 Fe(II): PAA at 5 µM each produce a spectrum almost identical to that of Fe(III), indicating rapid conversion of Fe(II) to Fe(III) in the presence of PAA. This is consistent with the fast OH production in Figure 6 and reaction 4. This reaction between Fe(II) and PAA is very rapid and previously unknown.

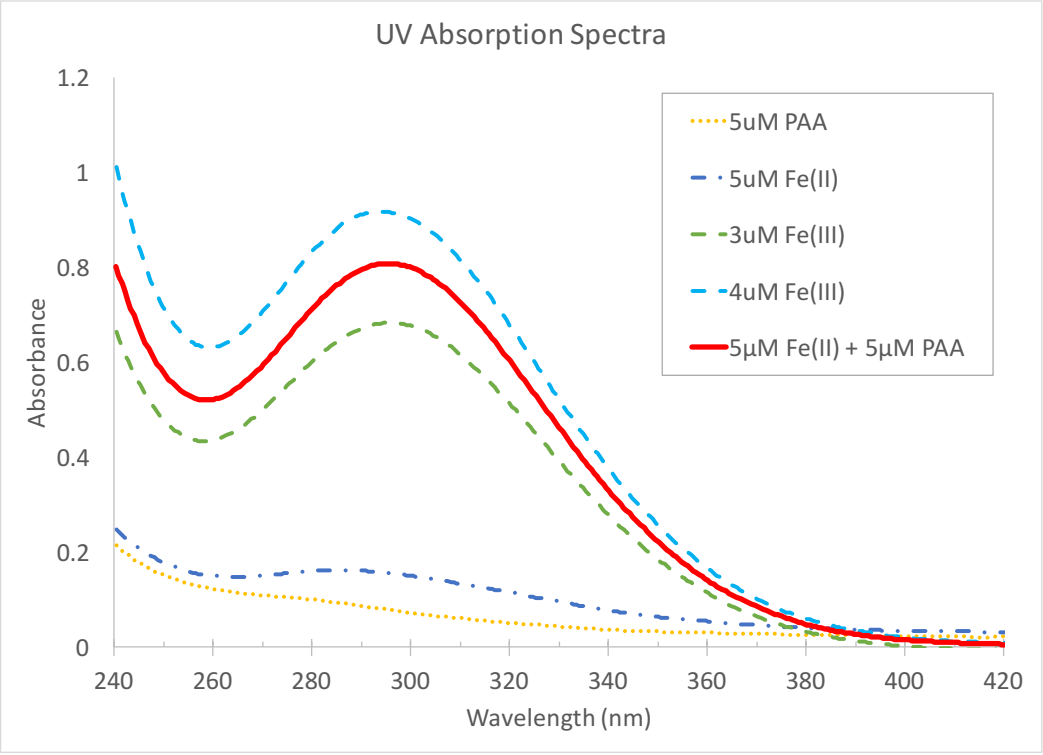

Figure 7. Absorbance of 5 µM each of peracetic acid (PAA) (5 µM, yellow*), Fe(II) from $FeSO_4$ (5 µM,* dark blue*), Fe(III) (from $FeCl_3$ at 3 and 4 µM), and mixtures of 1:1 Fe (II) ($FeSO_4$) + PAA (5 µM each), red line, in aqueous solution adjusted to pH = 3.5. After reacting for a few minutes, the 5 µM 1:1 mixture of Fe(II) and PAA results in an absorption spectrum identical to Fe(III), indicating the fast conversion of Fe(II) to Fe(III) and consistent with OH formation burst observed in Figure* 2.

Figure 8 shows the dependence of OH formation burst on the concentration of equal amounts of Fe(II) and PAA (1:1 ratio) reacting in the dark. Samples were measured in both the light and the dark immediately after being prepared, within one minute of sample mixing. As the concentrations of the two reactants increase, the molar yield of OH decreases.

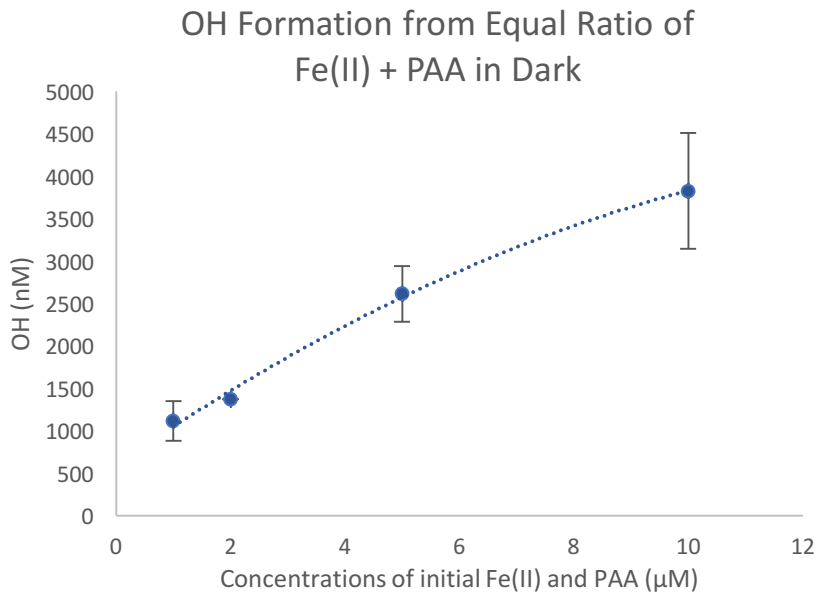

Figure 8. Concentration dependence of OH burst formation in the dark over the concentration range 1 – 10 µM. Samples were measured within 1 minute of being mixed. A quadratic polynomial is shown to guide the eye.

Figure 9 shows OH formation from solutions with 1 µM Fe(II) and 1, 5, and 10 µM PAA. Formation of OH in the light is at least double the formation in the dark for all cases. Additional PAA increases OH formation up to a point, after which does not seem to increase OH formation. In dark conditions with 1 µM Fe(II) and varying concentrations of PAA at 1, 5, and 10 µM, the OH "burst" is 1.11 ± 0.41 µM OH. Formation of OH in dark conditions appears to be roughly stoichiometric with Fe(II), consistent with a Fenton-like reaction.

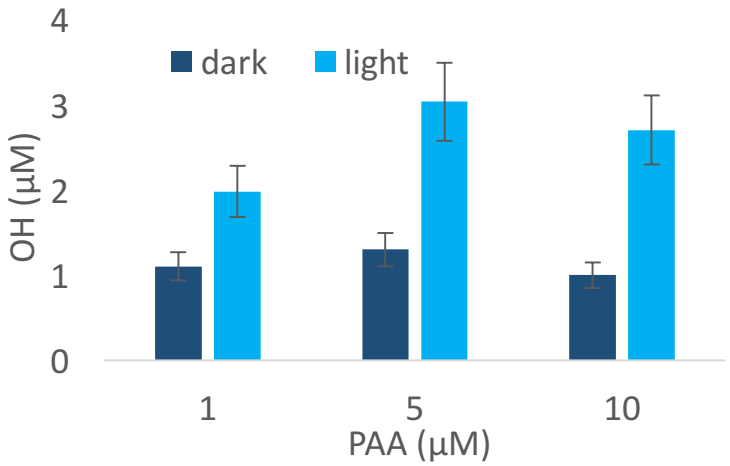

Figure 9. OH, formation in light (320 ± 10 nm) and dark from solutions of PAA and Fe(II) at pH 3.5 about 2 minutes after mixing. Initial Fe(II) was 1 μM for all measurements. (Paulson et al, 2019)

Initial OH formation from increasing concentrations of Fe(II) with 1, 5, and 10 μM PAA are shown in Figure 10. Solutions containing 1 μM PAA show no additional OH formed during the burst with a higher concentration of Fe(II), illustrated by the blue line in Figure 10. In solutions with a higher starting concentration of PAA (10 μM, gray line), increasing the concentration of Fe(II) does yield additional OH. While this is expected, the increase in OH compared to the increase in initial Fe(II) is not stoichiometric. Instead, about 0.61 μM OH is formed for each additional μM of Fe(II) added to the 10 μM PAA solution.

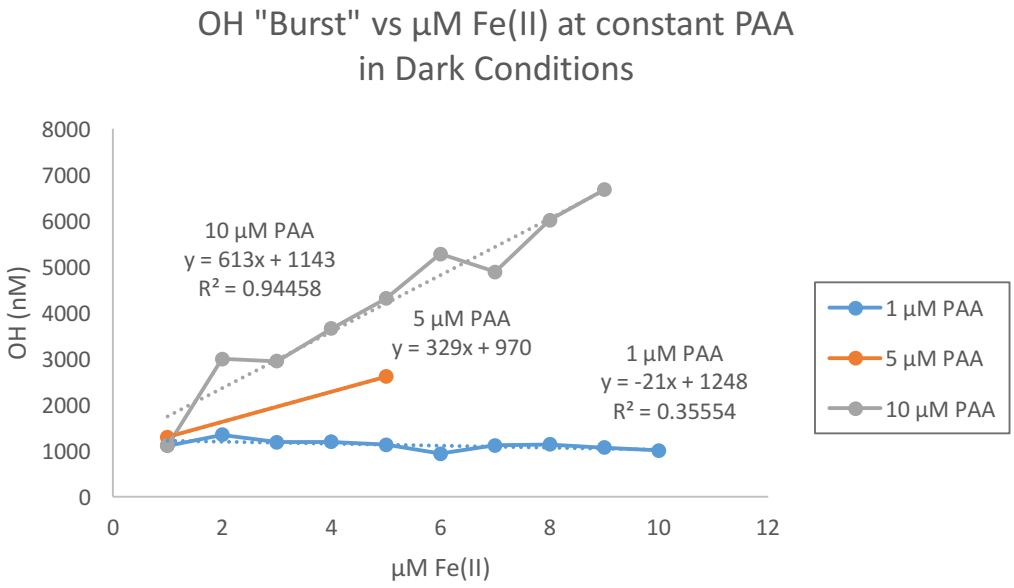

Figure 10. OH "burst". Initial OH formation in dark conditions from solutions of 1, 5, and 10 µM PAA and varying concentrations of Fe(II) at pH 3.5.

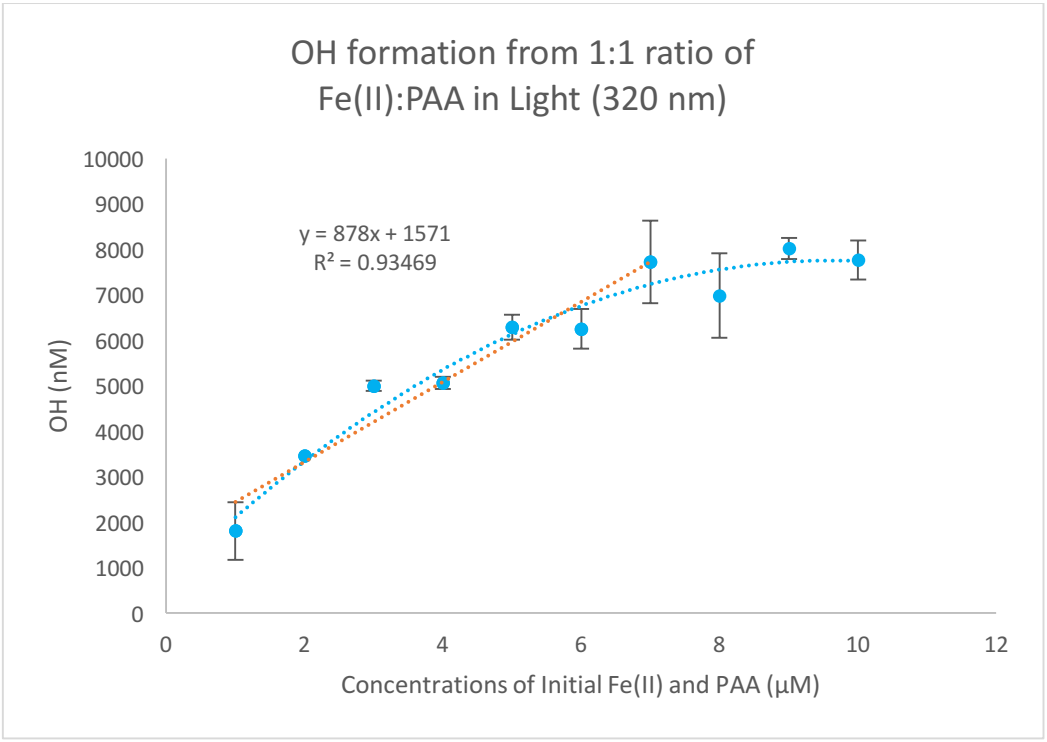

Figure 11 below shows the dependence of OH formation on the concentration of Fe(II) and PAA in presence of 320 nm light, with both reactants in a constant ratio. Compared to the 1:1 ratio

of Fe(II) to PAA in the dark (Figure 8), there is a similar overall trend with the molar yield decreasing as initial Fe(II) and PAA concentrations increase. This phenomenon may possibly result from complexes forming that limit further production of OH. In the presence of light, there is a higher OH burst averaging 1.61 ± 0.37 µM OH from 1 µM Fe(II) and PAA compared to the 1.14 ± 0.25 µM OH formed in the dark. The burst of OH from solutions in the presence of 320 nm light are consistently higher compared to those in the dark. For increasing concentrations at a 1:1 ratio of Fe(II) to PAA, the OH burst observed is 0.31 µM OH for each increasing µM of the reactants in dark conditions and 0.87 µM OH for each additional µM in the light.

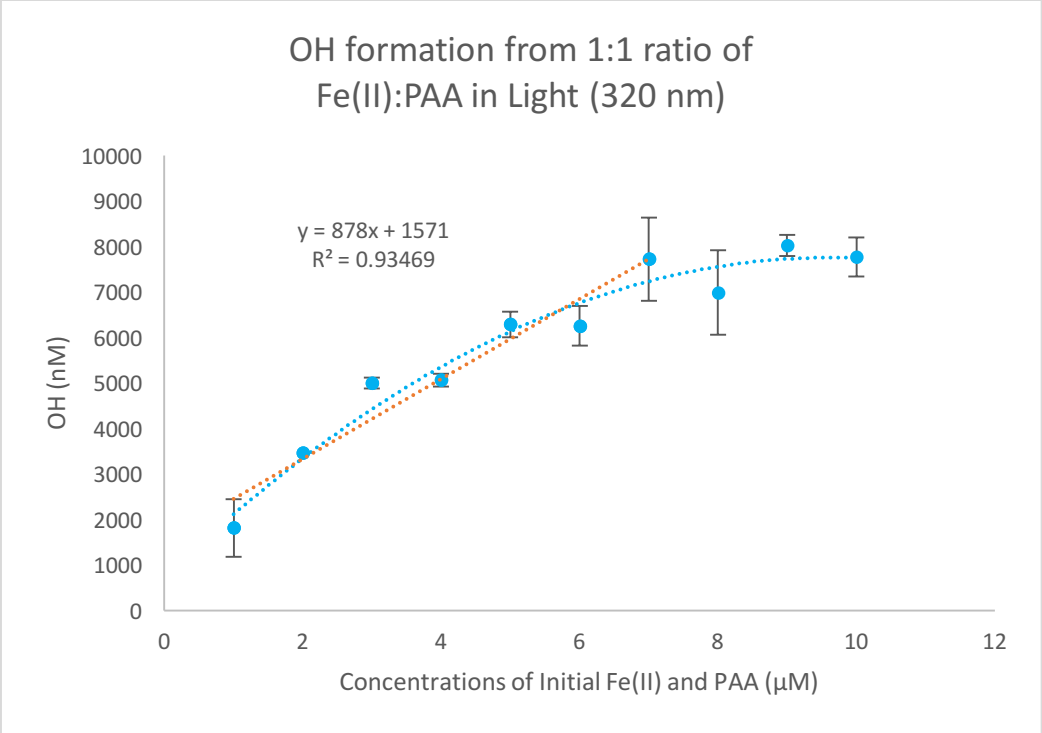

Figure 11. Concentration dependence of OH formation in 320 nm light in aqueous pH 3.5 solution over the concentration range 1-10 µM. Quadratic polynomial is shown to guide the eye. Orange line shows OH formation from concentration dependence up to 6 µM Fe(II) and PAA.

3.2 Inhibition of OH formation at higher concentrations of peractic acid and Fe(II)

A summary of average OH bursts produced from varying amounts of Fe(II) and PAA in light experiments is shown in Figure 12 below, with the color correlating to the concentration of the OH burst in nM. The OH burst is evident in the first measurement, which is taken immediately after the solution is mixed and within 30 seconds of the start of the reaction. Solutions containing iron concentrations of 9 μM and 10 μM with higher concentrations of PAA were excluded due to signal from the OH produced being close to saturation limit of the instrument. (Note: The fluorometer reaches saturation at 65535 fluorescence intensity (FI) units, and the hTA calibration standards used to quantify OH production remained linear up to 57000 – 60000 FI units, generally around 1800 nM hTA). Because of the linearity of the hTA calibration curve through high fluorescence intensities, we expect experiments in this range to be measureable. However, as the OH production fluorescence intensities approach saturation, it could be that the accuracy in measurements is not as good. Some experiments with high OH bursts could not be accurately measured and were not included in the summary below. This could also be a factor in the lower OH concentrations in Figure 11 at 9:9 and 10:10 μM of Fe(II) to PAA and the larger error bars at higher concentrations. For reference, fluorescence intensities for initial OH produced from 8 μM Fe(II) + 8 μM PAA in the light reached up to 89% of the saturation limit.

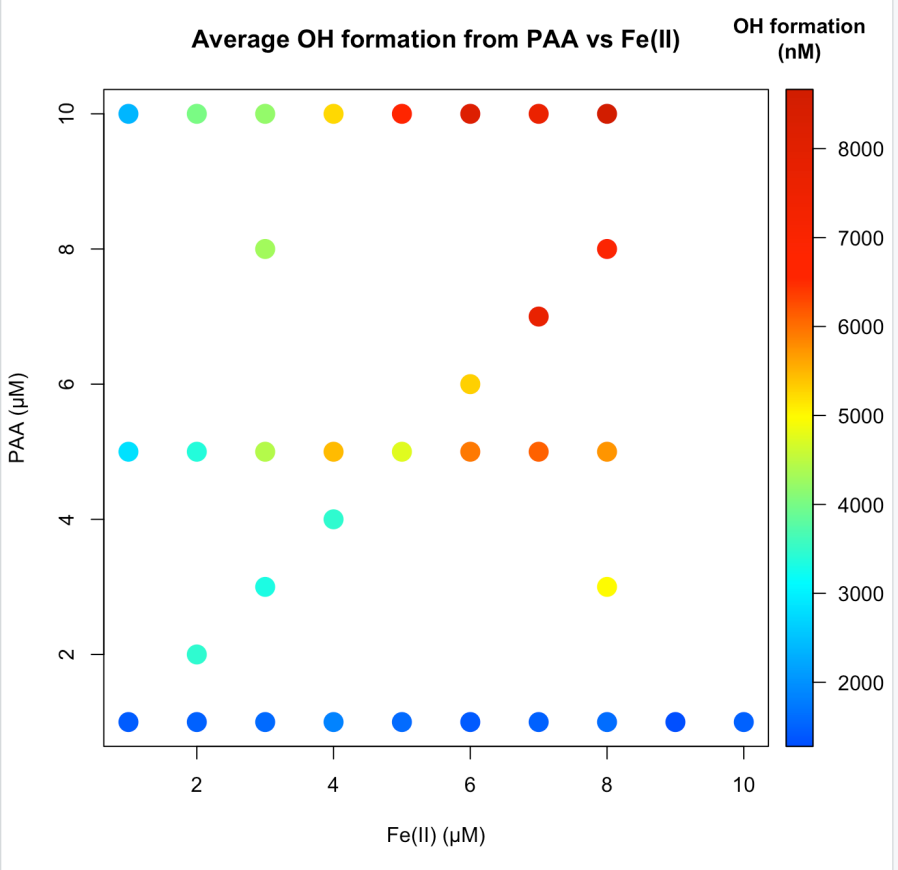

Figure 12. Color chart showing averaged OH bursts from PAA vs Fe(II) in 320 nm light.

From a stoichiometric standpoint, it might be expected that equal amounts of Fe(II) and PAA would produce similar amounts of OH, equal to or less than the lower concentration of the two reactants in the solution. For example, a solution containing 2 μM Fe(II) and 5 μM PAA might produce a maximum of 2 μM OH at the burst. Instead, average OH produced is around 3.39 μM. Looking at other solutions with less than 5 μM Fe(II) and either 5 or 10 μM PAA, there is more OH produced than the corresponding Fe(II) concentration. This could possibly indicate 'photo-Fenton' or light induced Fenton-like reactions are cycling Fe(II) to continuously react with the peracetic acid in solution. Looking at higher concentrations of the reactants, there does seem to be a limit to either the Fe(II) cycling or the reaction between Fe(II) and PAA thus inhibiting further

OH formation. The Figure 13 below shows the OH burst and the minimum concentration of either Fe(II) or PAA in solution. Again, OH formation following the concentration of the limiting reactant up to 7 µM; above 7µM evidence of inhibition or concentration-saturation effects are seen.

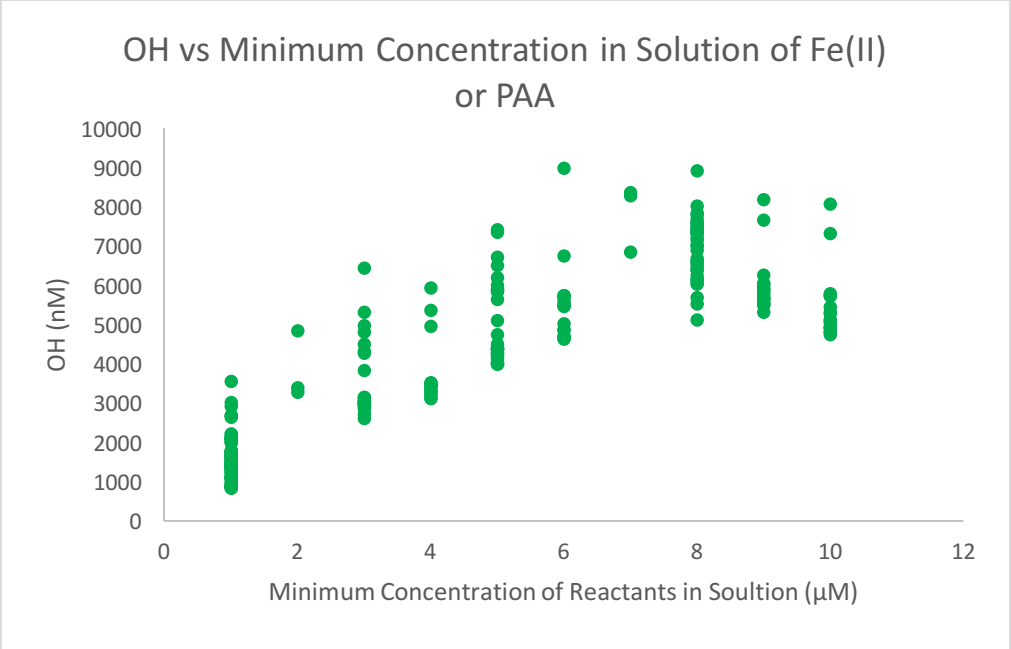

Figure 13. OH formation at the burst of reaction using the lower concentration between Fe(II) and PAA in the sample solution.

The OH burst is analyzed as a function of PAA concentration at constant Fe(II) values in Figure 14 below. The OH formation is dependent on Fe(II) and PAA concentrations but at high PAA concentrations OH formation yield decreases. OH yields are added as equations on the graph for the linear portion of OH formation. Higher Fe(II) concentration experiments appear to form less OH per µM of PAA.

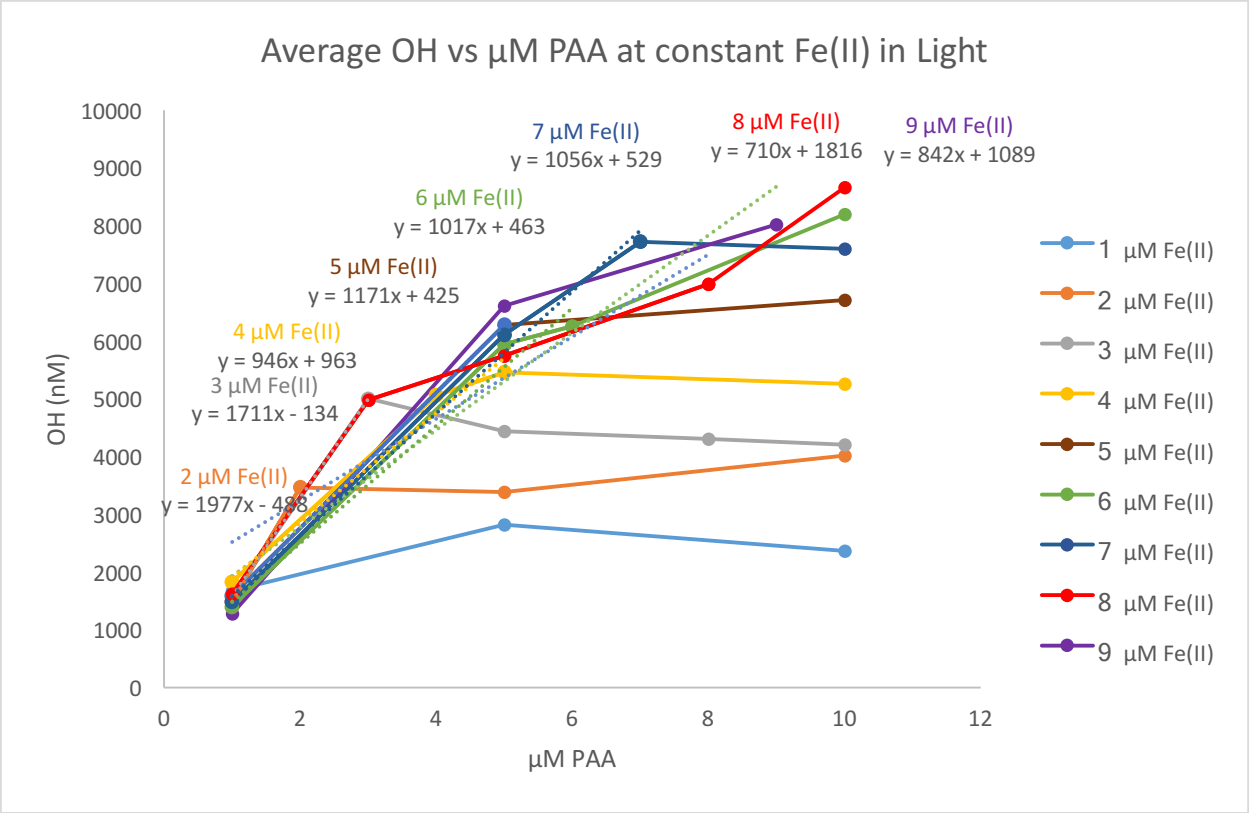

Figure 14. OH burst (nM) as a function of PAA (µM) at constant concentrations of Fe(II) in light.

In Figure 15, the dependence of OH formation on the ratio of Fe(II)-PAA in light conditions is analzyed from the first measurement of OH burst data for all experiments (same data used for Figure 14). Solutions with equal concentrations of Fe(II)-PAA have been excluded from this graph as their OH formation largely depends the initial concentrations. The ratio is defined as the concentration of Fe(II) to the total initial concentration of reactants in solution. A 1 µM Fe(II) and 5 µM PAA solution would then have a ratio of 1:6. On the x-axis, points closer to '0' represent solutions containing higher relative PAA concentrations, and values closer to '1' have more Fe(II) in them. A roughly parabolic trend is observed, with more OH produced when the reactants are closer to being equal in concentration.

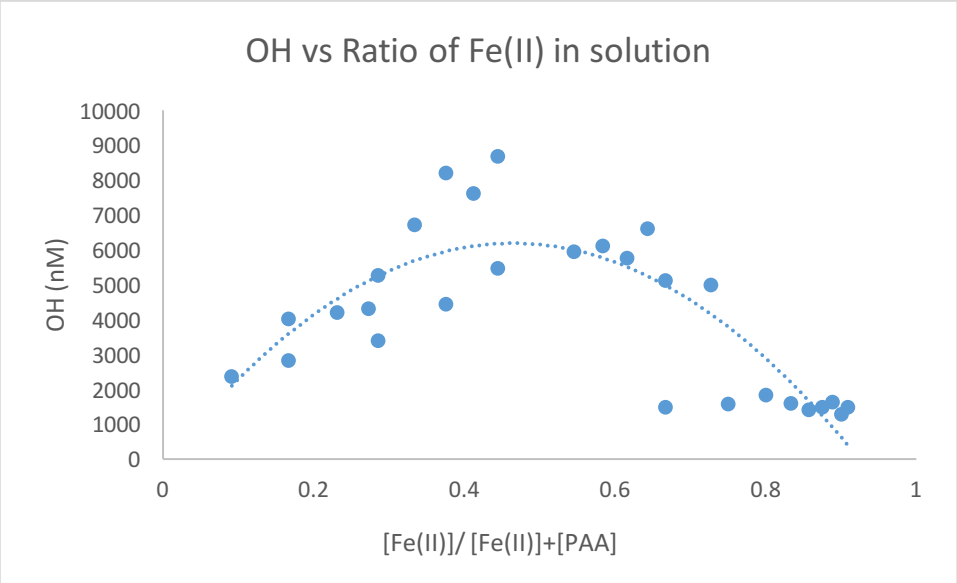

Figure 15. Relationship between ratio of Fe(II) in solution and OH formation. Ratio is defined as concentration of Fe(II) to the total concentration of reactants in solution initially.

Figure 16 below shows the OH burst from varying concentrations of Fe(II) with 5 and 10 µM of PAA. In solutions with 1 - 4 µM Fe(II) added, the amount of OH formed is similar despite doubling the initial PAA concentration. In the 5 µM PAA set, there is a leveling off of OH production after 5 µM of Fe(II) or more is in the solution. The 10 µM PAA set continues to increase OH production linearly as it approaches the 1:1 ratio. This is evidence that cycling of Fe(II) occurs immediately and the initial amount of Fe(II) in the solution will limit how much OH can be produced until the concentrations of Fe(II) and PAA are equal, where the reaction would then be limited by available PAA in solution.

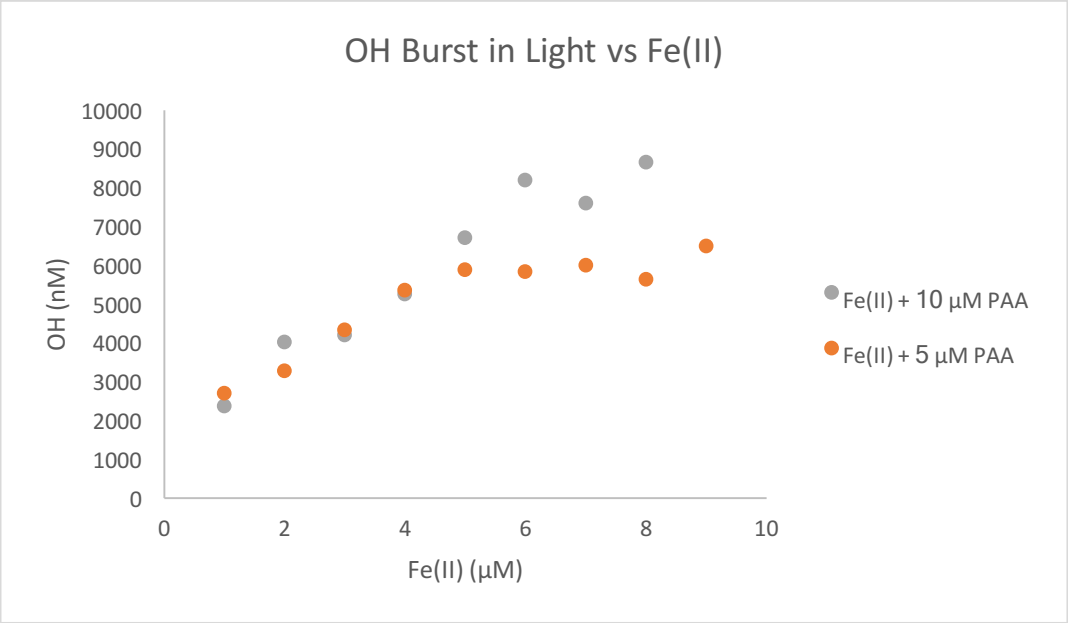

Figure 16. OH burst in light from 5 and 10 µM PAA with varying concentrations of Fe(II).

When considering if the Fe(II) or the PAA limits the formation of OH at higher concentration more is difficult to determine with the data available. Below, Figure 17 shows the OH formed per µM of reactant based on the slopes from Figure 14 and Figure 16 with the reactant being observed is held constant. More PAA data would be needed to explore the effects better.

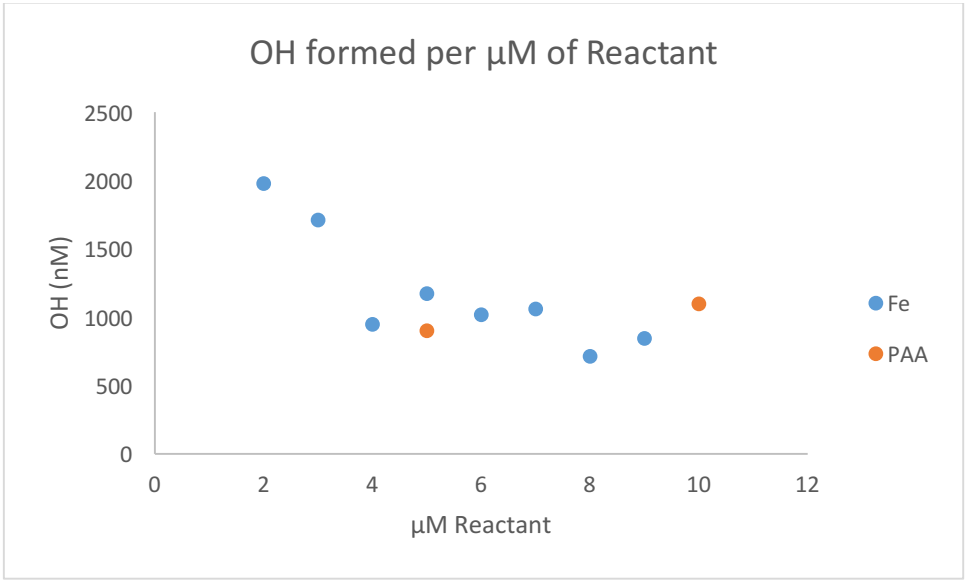

Figure 17. OH formed per µM of Reactant

The OH burst is highest when both reactants are present in the solution in equal amounts. Figure 18 below shows the OH burst from four solutions with different combinations of 3 or 8 μM initial concentrations of Fe(II) and PAA and a 1:1 μM Fe(II) to PAA positive control performed on the same day in 320 nm light. The combination of 3:3 had a burst of 6.45 μM OH which was triple the amount formed from the 1:1 solution (1.99 μM OH), but the 8:8 solution only produced slightly more than what was formed in the 3:3 solution with 7.80 μM OH. Solutions of 3 μM Fe(II) and 8 μM PAA or 8 μM Fe(II) and 3 μM PAA were expected to have a burst of OH equal to or larger than what was produced in the 3 μM Fe(II) and PAA solution because of the excess amount of reactants. However, both of these combinations (3:8 and 8:3) actually had less OH formation than when Fe(II) and PAA were in equal amounts at 3 μM. There appears to be a 'ratio effect' where solutions with an equal ratio of initial concentrations will have higher OH production than when initial concentrations are not equal. This could indicate the possibility of iron-organic complexes forming when there is an excess of one of the two in solution that are inhibiting OH production.

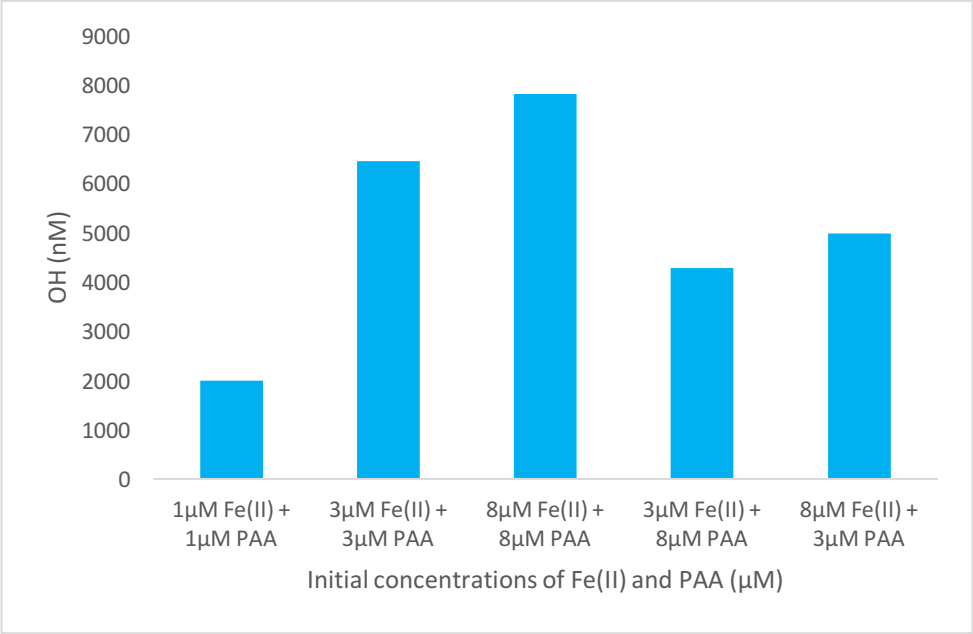

Figure 18. OH burst in light conditions at different combinations of 3 and 8 µM Fe(II) and PAA. A 1 µM Fe(II) and PAA solution was used as a positive control. All experiments were conducted on the same day in the same conditions.

3.3 Quantification of the OH burst in the presence of light

When quantifying how much OH is produced from the previously unknown reaction between Fe(II) and PAA in the presence of light, multiple factors should be considered. Both the concentration of initial reactants and the ratio between them are components of the reaction that will determine the yield of OH. To assess both and how these components may interfere with each other, we look at the OH formation as a function of the Fe(II) concentration in solutions with equal concentrations of Fe(II) and PAA (concentration effect) and the Fe(II) concentration relative to the total amounts of Fe(II) and PAA in solution (ratio effect).

The relationship between concentration of reactants and OH production is linear for most concentrations of equal Fe(II) and PAA up to 7 µM. After this, OH production levels off. Equations 1 and 2 show the empirical relationship from the data:

$$[OH] = f(Fe(II)) = 878[Fe(II)] + 1571 \qquad \text{(Equation 1)}$$

OH production as a function of the ratio of Fe(II) in solution follows a quadratic trend with highest production rates when [Fe(II)]~[PAA]. The empirical relationship is shown below, where x = [Fe(II)]/[Fe(II)]+[PAA]).

$$[OH] = f(z) = -29292x^2 + 27192x - 131 \qquad \text{(Equation 2)}$$

The overall yield of OH in the burst would be a function of both of these relationships,

$$[OH] = f(Fe(II)) + f(Fe/(Fe+PAA)) - C \text{ (Equation 3)}$$

with the following general functions for each component.

Concentration effect: $f(Fe(II))=m[Fe(II)]+b$

Ratio effect: $f(Fe/(Fe+PAA))=ax^2+bx+c$, *where* $x= Fe/(Fe+PAA)$

The concentration dependence and ratio dependence are not mutually exclusive, so OH formation cannot be easily separated and attributed to either of the effects. For this reason, a term 'C' has been added to Equation 3 above to represent the intersection of these two effects, which should be subtracted out. Because of the complexity of the system, a multivariate linear regression might be more appropriate for quantification.

3.3.1 Quantification using Multivariate Analysis

The ratio of Fe(II) to PAA and the concentration of Fe(II) in solution were chosen as predictor variables for OH formed, with the highest R^2 ($R^2 = 0.77$) compared to other combinations of variables, including minimum concentration of reactants, the sum of Fe(II) and PAA

concentrations, and using the ratio defined as amount of Fe(II) to total Fe(II) + PAA in solution. Multiple linear regression analysis was performed and coefficients were determined to give the following regression equation where $\hat{y}$ is the predicted OH, X_1 is the concentration of Fe(II) in solution and X_2 is the ratio of Fe(II) to PAA in solution.

$$\hat{y} = 0.56\,X_1 - 0.68\,X_2$$

While p values showed that these were statistically significant predictor variables, this regression is probably incorrect because the concentration of Fe(II) and ratio of Fe(II) to PAA do not have a linear relationship with OH formation. Predictions from this analysis are shown below.

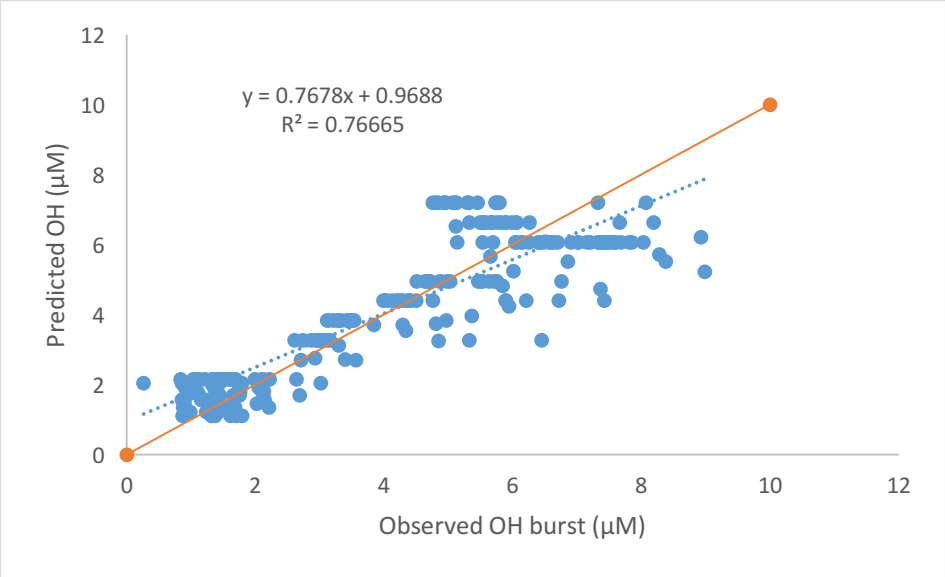

Figure 19. Predicted OH from multiple linear regression analysis using Fe(II) concentration and Fe:PAA ratio as predictor variables against observed OH values. Orange line y=x is added.

To better quantify and predict the OH, we attempted to characterize the relationships between our predictor variables and OH in a different way. Using data with equimolar concentrations of Fe(II) and PAA to determine the concentration effect on OH formation, we see linearity for concentrations up to 6 or 7 µM at which point the OH formation decreases. We believe

this trend follows the Michaelis-Menten curve fairly well, used often in enzyme kinetics and relates substrate concentration to reaction rate and demonstrates saturation effects. We adapt the Michaelis-Menten equation below, where $\widehat{OH}$ is the predicted OH formation, OH_{max} is the concentration of OH that is approached, X the concentration of Fe(II) or PAA, and b is a constant. The figure below shows the OH produced at the burst from equimolar concentrations of Fe(II) and PAA in blue, and the predicted OH concentrations from the Michaelis-Menten equation in orange.

$$Adapted\ M-M\ equation: \widehat{OH} = \frac{OH_{max}[X]}{b+[X]}$$

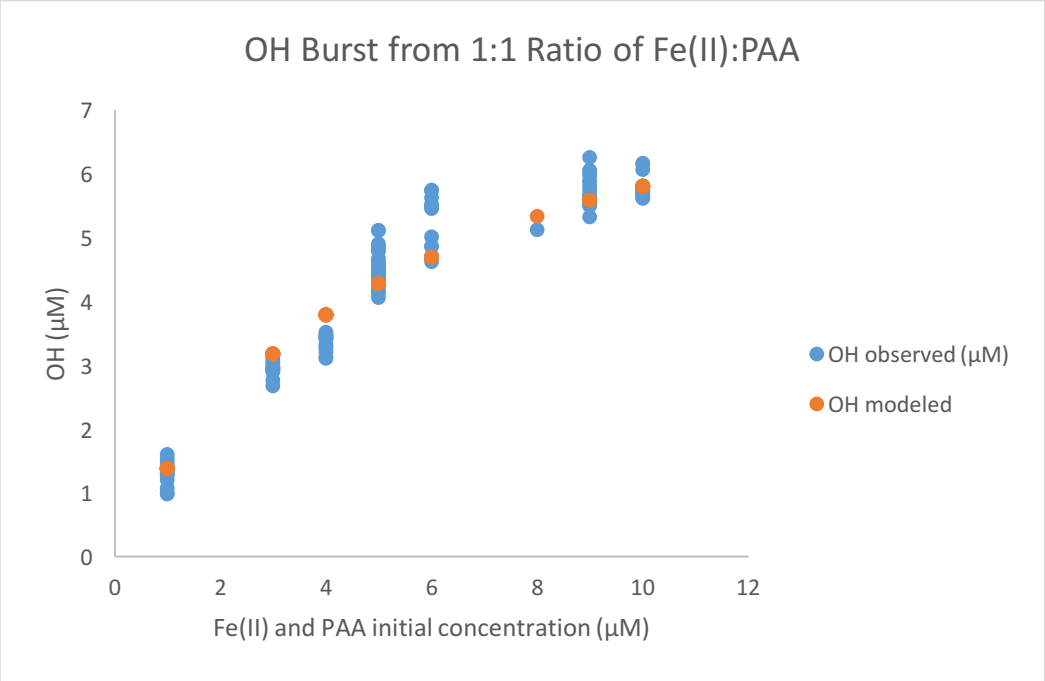

Figure 20. OH burst from equimolar concentrations of Fe(II) and PAA in solution in blue. OH is predicted from the adapted Michaelis-Menten equation shown in orange. The model follows the observed data reasonably well.

The Michaelis-Menten model follows the observed data fairly well. The Lineweaver-Burk equation is the linear form of the Michaelis-Menten equation found by taking its reciprocal shown

in the equation below. After manipulating the data to the Lineweaver-Burk equation, we get 1/OH as a predictor variable which represents the concentration effect shown in Figure 20. We represent the ratio effect by choosing the lower concentration of reactants (Fe(II) or PAA) in the solution because the reactant of lower concentration would be the limiting factor to OH production. These predictor variables chosen are now linear relationships, and we performed multivariate linear regression.

$$Adapted\ Lineweaver-Burk\text{:}\ \frac{1}{OH} = \frac{b}{OH_{max}} * \frac{1}{[X]} + \frac{1}{b}$$

The regression equation was obtained and is shown below. The predicted OH values were found by taking the inverse of results from the regression equation. Figure 21 shows the predicted OH concentration against the observed OH burst. The R^2 ($R^2 = 0.79$) for this analysis is slightly higher than our previous multivariate linear regression, but the predictor variable using the Linweaver-Burk is not statsitically significant (*p=0.96)*.

$$\widehat{OH} = 0.61X_1 + 0.002X_2 + 0.09$$

X_1 is the inverse of the limiting reactant concentration for the ratio effect and X_2 is the predicted inverse of OH from the Lineweaver-Burk equation for the concentration effect.

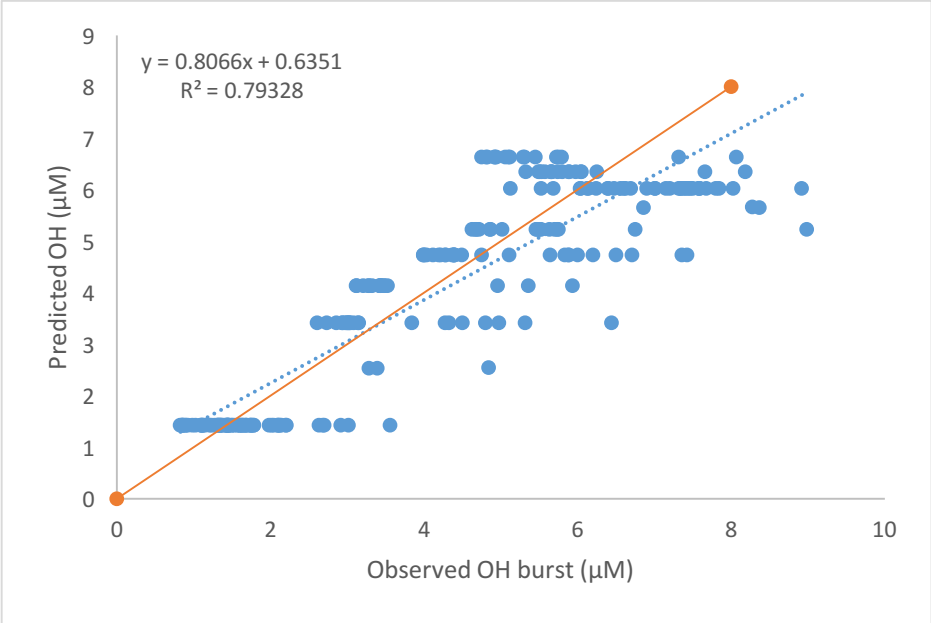

Figure 21 Predicted OH from multiple linear regression analysis using Lineweaver-Burk estimates and limiting reactant as predictor variables. Orange line y=x is added.

3.4 Interference of Additional Products with OH Probe

The potential interference of other, non-hydroxyl reaction products with terephthalate were considered for use of this probe in the PAA system. The terephthalate probe is widely accepted to be specefic to OH radicals (Fang et al, 1996; Gomes et al, 2005). Breakdown of peracetic acid may produce both OH radicals and acetyloxyl radicals and eventually methoxy radicals. Literature suggests alkoxy radicals do not prefer addition to allylic bonds, so a methoxy terephthalate is not expected to form (Walling, 1975; Das et al, 1981) and interference with our fluorescence measurements from these products is unlikely.

4. Conclusion

The decomposition of organic peroxides, commonly found in organic aerosols, in the presence of Fe(II) and potentially other transition metals is likely the source of the large OH burst

observed in ambient samples during simulated cloud formation done previously by Paulson's group. We could reproduce a similar burst in OH with a Fe(II)-PAA system at pH 3.5 in the presence of near UV light. The presence of light yielded substantially higher amounts of OH compared to the same reactions in the dark, indicating that the higher OH yield may be due to photo-Fenton like reactions.

The OH formation in the burst is dependent on concentrations of Fe(II) and PAA with evidence of possible inhibitory effects when the initial concentrations of these reactants are not in the solution at an equal ratio. At higher concentrations when molar yield of OH decreases, iron-organic complexes may be forming and limiting further OH production. This may also be ocurring when one of the two reactants in the system are in excess of the other.

This previously unknown, rapid metal-complex mediated formation of OH could be a substantial source of OH within cloud droplets and participate in the processing of organic aerosols. The Fe(II)-PAA system is complex; working to understand and quantify the system could help to improve the understanding of climate-relevant atmospheric droplet processes.

5. References

Abhishek, C., E. Barbara, G. Tarun, and T.S. N. (2016) Characterization of organic residues of size-resolved fog droplets and their atmospheric implications. Journal of Geophysical Research: Atmospheres, 121(8): 4317-4332. doi:10.1002/2015JD024508.

Arakaki, T. and B.C. Faust (1998) Sources, sinks, and mechanisms of hydroxyl radical (•OH) photoproduction and consumption in authentic acidic continental cloud waters from Whiteface Mountain, New York: The role of the Fe(r) (r = II, III) photochemical cycle. Journal of Geophysical Research: Atmospheres, 103(D3): 3487-3504. 10.1029/97JD02795.

Barnes, I., Hjorth, J., & Mihalopoulos, N. (2006). Dimethyl sulfide and dimethyl sulfoxide and their oxidation in the atmosphere. *Chemical Reviews*, *106*(3), 940-975.

Bianchi, F., Tröstl, J., Junninen, H., Frege, C., Henne, S., Hoyle, C. R., ... & Chen, X. (2016). New particle formation in the free troposphere: A question of chemistry and timing. *Science*, *352*(6289), 1109-1112.

Bianco, A., M. Passananti, H. Perroux, G. Voyard, C. Mouchel-Vallon, N. Chaumerliac, G. Mailhot, L. Deguillaume, and M. Brigante (2015) A better understanding of hydroxyl radical photochemical sources in cloud waters collected at the puy de Dôme station – experimental versus modelled formation rates. Atmos. Chem. Phys., 15(16): 9191-9202. 10.5194/acp-15-9191-2015.

Badali, K. M., Zhou, S., Aljawhary, D., Antiñolo, M., Chen, W. J., Lok, A., ... & Abbatt, J. P. D. (2015). Formation of hydroxyl radicals from photolysis of secondary organic aerosol material. *Atmospheric Chemistry and Physics*, *15*(14), 7831-7840.

Deguillaume, L., M. Leriche, K. Desboeufs, G. Mailhot, C. George, and N. Chaumerliac (2005) Transition metals in atmospheric liquid phases: Sources, reactivity, and sensitive parameters. Chemical Reviews, 105(9): 3388-3431.

Docherty, K. S., Wu, W., Lim, Y. B., & Ziemann, P. J. (2005). Contributions of organic peroxides to secondary aerosol formed from reactions of monoterpenes with O3. *Environmental science & technology*, *39*(11), 4049-4059.

Ehn, M., Thornton, J. A., Kleist, E., Sipilä, M., Junninen, H., Pullinen, I., ... & Lopez-Hilfiker, F. (2014). A large source of low-volatility secondary organic aerosol. *Nature*, *506*(7489), 476.

El-Sayed, M.H., Y. Wang, and C.J. Hennigan (2015) Direct atmospheric evidence for the irreversible formation of aqueous secondary organic aerosol. Geophysical Research Letters, 42(13): 5577-5586. doi:10.1002/2015GL064556.

Ervens, B., A. Sorooshian, Y.B. Lim, and B.J. Turpin (2014) Key parameters controlling OH-initiated formation of secondary organic aerosol in the aqueous phase (aqSOA). Journal of Geophysical Research: Atmospheres, 119(7): 3997-4016. 10.1002/2013JD021021.

Faust, B. C., Powell, K., Rao, C. J., and Anastasio, C.: Aqueousphase photolysis of biacetyl, and a source of acetic acid, peroxyacetic acid, hydrogen peroxide, and the highly oxidizing peroxyacetyl radical in aqueous aerosols, fogs, and clouds, Atmos. Environ., 31, 497–510, 1997.

Finlayson-Pitts, B.J. and J. Pitts, *Chemistry of the Upper and Lower Atmosphere*. 1st ed. 2000, San Diego, London: Academic Press.

Ge, X., Q. Zhang, Y. Sun, C.R. Ruehl, and A. Setyan (2012) Effect of aqueous-phase processing on aerosol chemistry and size distributions in Fresno, California, during wintertime. Environmental Chemistry, 9(3): 221-235.

Gligorovski, S., Strekowski, R., Barbati, S., & Vione, D. (2015). Environmental implications of hydroxyl radicals (• OH). *Chemical Reviews*, *115*(24), 13051-13092.

Gonzalez, D. H., Kuang, X. M., Scott, J. A., Rocha, G. O., & Paulson, S. E. (2018). Terephthalate Probe for Hydroxyl Radicals: Yield of 2-Hydroxyterephthalic Acid and Transition Metal Interference. *Analytical Letters*, *51*(15), 2488-2497.

Gonzalez, D. H., Cala, C. K., Peng, Q., & Paulson, S. E. (2017). HULIS enhancement of hydroxyl radical formation from Fe (II): Kinetics of fulvic acid–Fe (II) complexes in the presence of lung antioxidants. *Environmental science & technology*, *51*(13), 7676-7685.

Herrmann, H., Hoffmann, D., Schaefer, T., Bräuer, P., & Tilgner, A. (2010). Tropospheric aqueous-phase free-radical chemistry: Radical sources, spectra, reaction kinetics and prediction tools. *ChemPhysChem*, *11*(18), 3796-3822.

Hoffmann, E. H., Tilgner, A., Schroedner, R., Bräuer, P., Wolke, R., & Herrmann, H. (2016). An advanced modeling study on the impacts and atmospheric implications of multiphase dimethyl sulfide chemistry. *Proceedings of the National Academy of Sciences*, *113*(42), 11776-11781.

Isaksen, I. S. A., & Dalsøren, S. B. (2011). Getting a better estimate of an atmospheric radical. *Science*, *331*(6013), 38-39.

Jimenez, J. L., Canagaratna, M. R., Donahue, N. M., Prevot, A. S. H., Zhang, Q., Kroll, J. H., ... & Aiken, A. C. (2009). Evolution of organic aerosols in the atmosphere. *Science*, *326*(5959), 1525-1529.

Lelieveld, J., Butler, T. M., Crowley, J. N., Dillon, T. J., Fischer, H., Ganzeveld, L., ... & Williams, J. (2008). Atmospheric oxidation capacity sustained by a tropical forest. *Nature*, *452*(7188), 737.

Levy II, H. (1972). Photochemistry of the lower troposphere. *Planetary and Space Science*, *20*(6), 919-935.

Lightfoot, P. D., Cox, R. A., Crowley, J. N., Destriau, M., Hayman, G. D., Jenkin, M. E., ... & Zabel, F. (1992). Organic peroxy radicals: kinetics, spectroscopy and tropospheric chemistry. *Atmospheric Environment. Part A. General Topics*, *26*(10), 1805-1961.

Lim, H.-J., A.G. Carlton, and B.J. Turpin (2005) Isoprene Forms Secondary Organic Aerosol through Cloud Processing: Model Simulations. Environmental Science & Technology, 39(12): 4441-4446. 10.1021/es048039.

Lind, J. A., Lazrus, A. L., and Kok, G. L.: Aqueous phase oxidation of sulfur by hydrogen peroxide and methyl hydroeroxide and peroxyacetic acid, J. Geophys. Res., 92, 4171–4177, 1987.

Lu, K., Guo, S., Tan, Z., Wang, H., Shang, D., Liu, Y., ... & Zhang, Y. (2018). Exploring atmospheric free-radical chemistry in China: the self-cleansing capacity and the formation of secondary air pollution. *National Science Review*.

Paulot, F., Crounse, J. D., Kjaergaard, H. G., Kürten, A., Clair, J. M. S., Seinfeld, J. H., & Wennberg, P. O. (2009). Unexpected epoxide formation in the gas-phase photooxidation of isoprene. *Science*, *325*(5941), 730-733.

Paulson, S. E., Gallimore, P. J., Kuang, X. M., Chen, J. R., Kalberer, M., & Gonzalez, D. H. (2019). A light-driven burst of hydroxyl radicals dominates oxidation chemistry in newly activated cloud droplets. *Science advances*, *5*(5), eaav7689.

Sekiguchi, M., Nakajima, T., Suzuki, K., Kawamoto, K., Higurashi, A., Rosenfeld, D., ... & Mukai, S. (2003). A study of the direct and indirect effects of aerosols using global satellite data sets of aerosol and cloud parameters. *Journal of Geophysical Research: Atmospheres*, *108*(D22).

Seinfeld, J. H., & Pandis, S. N. (2016). *Atmospheric chemistry and physics: from air pollution to climate change*. John Wiley & Sons.

Staffelbach, T. A., Orlando, J. J., Tyndall, G. S., & Calvert, J. G. (1995). The UV-visible absorption spectrum and photolysis quantum yields of methylglyoxal. *Journal of Geophysical Research: Atmospheres*, *100*(D7), 14189-14198.

Riva, M. (2016). Multiphase chemistry of highly oxidized molecules: the case of organic hydroperoxides. *Chem*, *1*(4), 526-528.

Tong, H., Lakey, P. S., Arangio, A. M., Socorro, J., Kampf, C. J., Berkemeier, T., ... & Shiraiwa, M. (2017). Reactive oxygen species formed in aqueous mixtures of secondary organic

aerosols and mineral dust influencing cloud chemistry and public health in the Anthropocene. *Faraday discussions*, *200*, 251-270.

Tong, H., Arangio, A. M., Lakey, P. S. J., Berkemeier, T., Liu, F., Kampf, C. J., ... & Shiraiwa, M. (2015). Hydroxyl radicals from secondary organic aerosol decomposition in water. *Atmospheric Chemistry & Physics Discussions*, *15*(21).

Voulgarakis, A., Naik, V., Lamarque, J. F., Shindell, D. T., Young, P. J., Prather, M. J., ... & Cionni, I. (2013). Analysis of present day and future OH and methane lifetime in the ACCMIP simulations. *Atmospheric Chemistry and Physics*, *13*(5), 2563-2587.

Welch, K. D., Davis, T. Z., & Aust, S. D. (2002). Iron autoxidation and free radical generation: effects of buffers, ligands, and chelators. *Archives of biochemistry and biophysics*, *397*(2), 360-369.

Whalley, L. K., Stone, D., George, I. J., Mertes, S., Van Pinxteren, D., Tilgner, A., ... & Heard, D. E. (2015). The influence of clouds on radical concentrations: observations and modelling studies of HO x during the Hill Cap Cloud Thuringia (HCCT) campaign in 2010. *Atmospheric Chemistry and Physics*, *15*(6), 3289-3301.

Zellner, R., M. Exner, and H. Herrmann (1990) Absolute OH quantum yields in the laser photolysis of nitrate, nitrite and dissolved H2O2 at 308 and 351 nm in the temperature range 278–353 K. Journal of Atmospheric Chemistry, 10(4): 411-425. 10.1007/bf00115783.

Zepp, R.G., B.C. Faust, and J. Hoigne (1992) Hydroxyl radical formation in aqueous reactions (pH 3-8) of iron(II) with hydrogen peroxide: the photo-Fenton reaction. Environmental Science & Technology, 26(2): 313-319. 10.1021/es00026a011.

Zhang, X., Chen, Z. M., He, S. Z., Hua, W., Zhao, Y., & Li, J. L. (2010). Peroxyacetic acid in urban and rural atmosphere: concentration, feedback on PAN-NO x cycle and implication on radical chemistry. *Atmospheric Chemistry and Physics*, *10*(2), 737-748.